Effect of hydroxypropyl methylcellulose and aggregate volume on fresh and hardened properties of 3D printable concrete

Kaya, Ebru; Ciza, Baraka; Yalçınkaya, Çağlar; Felekoğlu, Burak; Yazıcı, Halit; Çopuroğlu, Oğuzhan

DOI
10.1016/j.conbuildmat.2024.139253

Publication date
2024

Document Version
Final published version

Published in
Construction and Building Materials

Construction and Building Materials 456 (2024) 139253

Contents lists available at ScienceDirect

Construction and Building Materials

journal homepage: www.elsevier.com/locate/conbuildmat

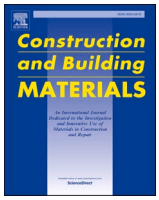

Effect of hydroxypropyl methylcellulose and aggregate volume on fresh and hardened properties of 3D printable concrete

Ebru Kaya [a,b], Baraka Ciza [a,b], Çağlar Yalçınkaya [b,*], Burak Felekoğlu [b], Halit Yazıcı [b], Oğuzhan Çopuroğlu [c]

[a] The Graduate School of Natural and Applied Sciences, Dokuz Eylül University, İzmir, Türkiye
[b] Department of Civil Engineering, Faculty of Engineering, Dokuz Eylül University, İzmir, Türkiye
[c] Microlab, Section Materials and Environment, Faculty of Civil Engineering and Geosciences, Delft University of Technology, Delft, The Netherlands

ARTICLE INFO

Keywords:
3D concrete printing
Aggregate volume
Viscosity modifying admixtures
Green strength
Ram extrusion

ABSTRACT

Three-dimensional (3D) concrete printing necessitates a balance between various ingredients of the mix composition. This study investigated the effect of hydroxypropyl methylcellulose (HPMC) dosage at various aggregate volumes on fresh, rheological, and mechanical properties of 3D printable concrete (3DPC). Accordingly, 3DPC mixtures having three aggregate volumes, namely 44, 41, and 38 %, were produced at a constant water-to-binder ratio. For each aggregate volume, three HPMC dosages, namely 0, 0.14, and 0.28 % by weight of cement, were studied. A mini-slump flow table and a manual printing gun were used to assess the flow diameter and printability. Rheological properties were determined using a rotational rheometer and extrusion device. The buildability was assessed through green strength testing. Results showed a directly proportional relationship between HPMC dosage and fresh and rheological properties of these mixtures. At a constant w/c ratio, increasing the aggregate volume led to higher green strength and extrusion pressure at all piston-moving velocities. Overall, at an early age, the effect of HPMC dosage was more significant on the static yield stress of mixtures with lower paste volume while being more accentuated on the green strength for mixes with higher paste volume. The positive impact of increasing HPMC dosage on the green strength becomes insignificant at later ages. The effect of increasing HPMC dosage, however, was more pronounced on the extrudability of mixtures with higher paste volume by preserving their extrudability at later ages. Finally, HPMC addition led to strength losses of up to 28.63 and 32.7 % for flexural and compressive strength, respectively.

1. Introduction

Three-dimensional concrete printing (3DCP) brings digitalization and automation to the construction industry [1,2]. As an alternative to conventional manual-based techniques, it holds great potential to revolutionize concreting processes by compensating for the shortage of skilled labor, improving workspace safety, as well as lowering construction costs and time [3]. Most importantly, formwork-free construction facilitates the creation of complex geometric shapes with topological optimization while also minimizing construction-related wastes, ultimately benefiting the environment [4,5].

Cement-based object fabrication without formwork demands finding harmony between cement-based mix and printing requirements. Extrudability, printability window, and buildability are the main stages of 3D printing operations [6]. Extrudability can be defined as the capacity of a mix to be continuously extruded through the nozzle without cracking, discontinuities, or clogging. It has been determined that the extrudability of a mix is directly related to its static yield stress and plastic viscosity, which are rheological characteristics commonly determined with the help of shear-based rheometers by employing specific measurement methods [7,8].

Since extrusion is realized by pumping, it has been observed that a lower static yield stress and plastic viscosity are preferable. However, a relatively higher static yield stress is required for the extruded filament to maintain its shape in the absence of molds against its own weight, and the shear stress induced by gravity. Previous studies have referred to this feature as shape stability [7,9]. Therefore, the determination of rheological behaviors of 3D printable concrete (3DPC) with the help of shear-based rheometers might provide misleading results. Previous studies have reported the occurrence of the slip wall effect or capacity

* Corresponding author.
E-mail address: caglar.yalcinkaya@deu.edu.tr (Ç. Yalçınkaya).

https://doi.org/10.1016/j.conbuildmat.2024.139253
Received 28 February 2024; Received in revised form 2 October 2024; Accepted 14 November 2024
Available online 23 November 2024

deficiency in the case of highly concentrated suspensions or mixtures with high thixotropic behavior [10]. Hence, a great deal of studies have alternatively employed ram extrusion tests in the characterization of rheological properties of 3D printable mixtures [10,11]. The time-dependent hydration process of cement-based mixtures leads to the loss of fluidity and, subsequently, stiffening. To characterize the time-span during which a mix retains its desired printability, the terms "printing window" or "printing open time" have been used. It has been determined that the printing window is directly associated with the rate of yield stress evolution to the stage where the mix becomes non-extrudable [12,13]. Hence, various mix ingredients such as viscosity-modifying materials may affect the printability window differently. The term buildability has been employed to indicate the ability of a layer to retain its shape and the weight of layers stacked in the process up to a certain height. Printability window and buildability depend on the thixotropic characteristics of mixtures and have been studied through different indirect methods such as displacement-controlled green strength and penetration tests [10,14].

Yalçınkaya [5] investigated the effect of HPMC dosage on the hydration kinetics and hydrated properties of 3DPC. It was reported that the use of HPMC led to air entrainment and lower strength development at 28 days [5]. Similarly, Figueiredo et al. [15] investigated the effect of HPMC on the hydration and microstructure of cement pastes. They found that while HPMC caused set retardation of these mixtures, it led to the loss in compressive strength through air entraining. Chen et al. [16] studied the effect of calcined clay with various metakaolin content on the fresh and hardened properties of 3D printable mixtures developed using Ordinary Portland cement and limestone. They concluded that calcined clay not only enhanced the early properties of these mixtures by improving their thixotropy, but also their hardened properties by densifying the matrix [17]. Mohan et al. [18] investigated the effect of various aggregate volumes on the rheological properties of high thixotropic concrete mixtures. They reported that while the increase in binder volume led to a rise in static yield stress and plastic viscosity, it decreased the structuration rate. Similarly, they found a directly proportional relationship between the sand-to-binder ratio and rheological properties of 3D printable mixtures, namely the static yield stress and plastic viscosity. Regarding the sand-to-binder ratio, various studies have noted the necessity of a higher binder volume in 3D printable mixtures than that of conventional or other particular concrete types [6]. Consequently, 3DPC is more prone to shrinkage cracks due to a lower sand-to-binder ratio and lack of formwork. Furthermore, it has been found that the curing environment also affects the shrinkage behavior of this concrete type [19].

The literature review shows that the effect of HPMC on the rheological and hardened properties of 3DPC has been extensively studied at constant aggregate volumes. Additionally, a few studies have been performed to investigate the effect of various aggregate volumes on the properties of 3DPC at constant HPMC dosages. However, no studies have been conducted to assess the impact of various dosages of HPMC at different aggregate volumes on the rheological, fresh, and mechanical properties of 3DPC. Hence, the present study aimed to experimentally investigate the combined effect of various HPMC dosages at different aggregate volumes on the rheological, fresh, and mechanical properties of 3DPC. Accordingly, 3DPC mixtures having three different aggregate volumes have been produced at a constant water-to-binder ratio. Additionally, for each aggregate volume, three different dosages of HPMC were studied.

2. Materials and method

2.1. Materials

In the present study, the production of 3DPC samples was realized by utilizing CEM I 42.5 R type Portland cement (PC). Its particle size distribution determined by a laser size analyzer is given in Fig. 1.

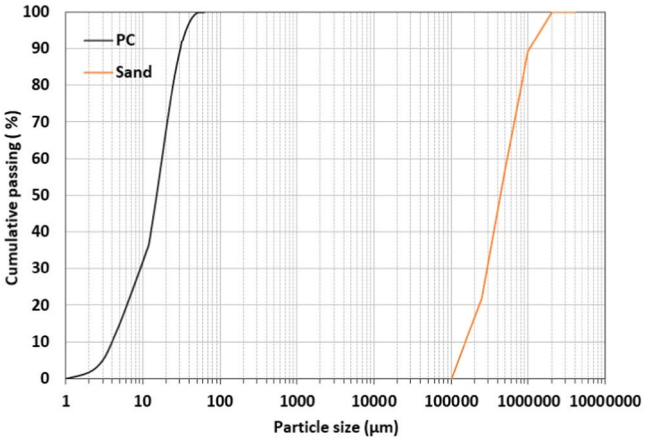

Fig. 1. The particle size distribution of PC and sand.

Additionally, a hydroxypropyl methylcellulose (HPMC) based viscosity modifying agent (VMA) in powder form having a viscosity of 55.000–85.000 mPa.s was used to enhance the early strength and buildability of the developed mixtures. A polycarboxylate ether-based high-range water-reducing admixture (HRWRA) in aqueous form (brand name: ACE 450) was used to adjust the workability of the mixtures. The properties of this superplasticizer (SP) are given in Table 1. Natural river sand with a maximum particle size of 2 mm was used as aggregate. Its particle size distribution is presented in Fig. 1. The utilized sand had a specific gravity, water absorption capacity, and fineness modulus of 2.46, 0.67 %, and 1.3, respectively. Finally, tap water was used as mixing water.

2.2. Methods

2.2.1. Mixing procedure

The mixing procedure employed in the preparation of 3DPC mixtures of the present study is schematically summarized in Fig. 2. A Hobart mixer type was used during mixing. Two mixing speeds, namely low and high, corresponding to 60 and 120 rpm, respectively, were employed. As can be seen from Fig. 2, Portland cement and sand were initially mixed at low speed for 2 minutes. Afterward, 70 % of the mixing water was added while mixing at low speed, and the mixing was carried on for another 2 minutes. Subsequently, a pre-prepared mixture of HRWRA and 30 % of the mixing water was added, and the mixing was elongated for a further 3 minutes. HPMC was then added into the mix and continued mixing at low speed for an additional 3 minutes. Finally, 3 minutes of mixing at high speed was employed. Hence, the mixing procedure took a total of 13 minutes.

2.2.2. 3D printable mixture development

Previous studies have successfully established various test methods to assess different symbolical features (i.e., shape stability, extrudability, and buildability) required for 3DPC. With the help of these test methods, the developed mixtures can be classified as 3D printable and suitable for further tests. Accordingly, in the present study, various test methods in accordance with previous literature have been used to

Table 1
Properties of the used superplasticizer.

Properties	Explanations
Form	Liquid
Structure of materials	Polycarboxylic ether-based
Color	Amber
pH value	5 – 7 (20 °C)
Density	1.069 – 1.109 kg/L (20 °C)
Solubility in water	Miscible

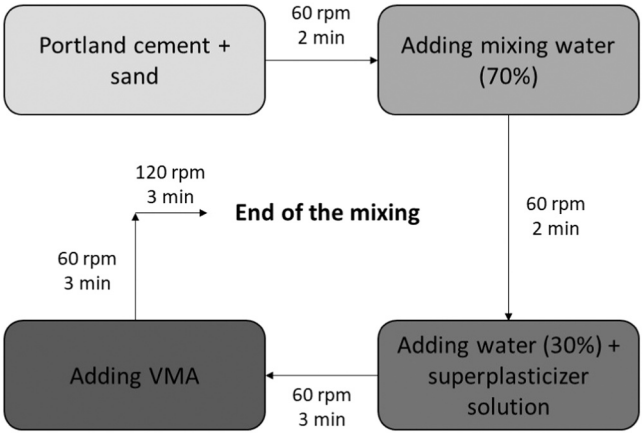

Fig. 2. Mixing procedure.

develop 3D printable mixtures.

Many studies have demonstrated the correlation of the flow diameter of cementitious composites to the shape stability required of 3D printable mixtures. It has been reported that satisfactory shape stability corresponds to a flow diameter ranging between 140 and 190 mm. For similar purposes, the standard flow table test according to ASTM 1437–20 [20] was used to assess the shape stability of the developed mixtures. Moreover, it was found that good extrudability and satisfactory buildability of 3D printable mixtures can be indirectly evaluated by analyzing the quality of a printed filament using a manual injection gun [21]. They reported that good extrudability can be correlated with printing a single filament at a length of 300 mm without any discontinuities. Additionally, this printed filament can be used to assess the shape stability by measuring its width at three different regions. Accordingly, adequate shape stability corresponds to a width that is less than 10 % wider than that of the nozzle, as well as maintaining a diameter uniformity all over its length. Furthermore, they determined that satisfactory buildability can be assessed by measuring the deformation of the bottom layer after continuously stacking five layers at zero printing intervals. They concluded that a deformation of the bottom layer equaling or less than 25 % denoted good buildability. For this purpose, a manual injection gun presented in Fig. 3 was used to print filaments at a printing speed of 5 mm/s. As a result of these experiments, only mixtures meeting all these requirements were selected for further tests.

2.2.3. Flowability and setting times

Fresh mortars were assessed immediately at the end of the mixing procedure by performing a standard flow table test following ASTM 1437–20 [20] The initial and final setting times were measured per TS EN 480–2 [22] using an automatic Vicat apparatus.

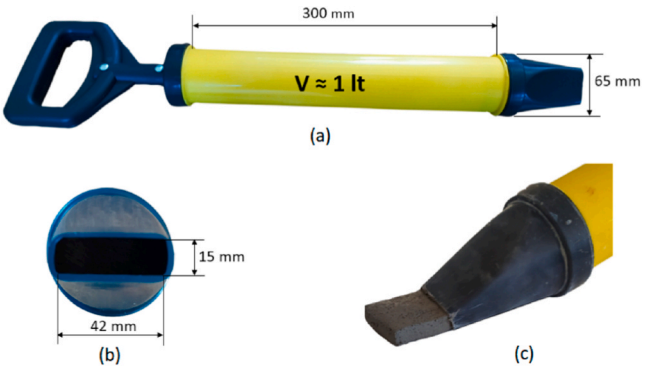

Fig. 3. Mortar injection gun (a), the dimensions of the nozzle (b), and extrusion process (c) [5].

2.2.4. Extrusion test

2.2.4.1. Extrusion at varying material age with constant extrusion speed. A custom-made ram extruder, as in the study by Chen et al. [10] and Zhou et al. [23], was designed and employed to study the effect of material age on the extrudability of 3DPC composites. The utilized ram extruder is presented in Fig. 4. As can be seen, it consisted of four pieces namely a piston, barrel, nozzle, and a stand. The dimension of each piece is given in Table 2. The testing method employed is schematically summarized in Fig. 4. The testing method consisted of four different regions. The first region (L_1) from 0 to 50 mm corresponded to a region where the piston moved freely before coming in contact with the material in the barrel. The second region (L_2) from 50 to 90 mm corresponded to a region where the piston moved inside the barrel in contact with the material. In this region, the flow of the material through the nozzle does not take place, and the region is called the compaction zone. The third zone (L_3), utilized as the measuring zone, ranges between 90 and 130 mm. Here, the material starts flowing through the nozzle. The last zone (L_4 or L_{dz}), known as the dead zone, ranges from 130 to 170 mm. The dead zone changes in accordance with the dimensions of the barrel and can be calculated using Eq. 1. The existence of this zone was studied and reported by Basterfield et al. [24]. In this equation, $\varnothing_{max}$ represents the maximum convergent flow angle of paste-like materials, which has been reported in previous studies to be in the range of 40–60 degrees.

$$L_{dz} = \frac{D_o - D}{2\tan\varnothing_{max}} \quad (1)$$

Here, Do is the diameter of the barrel, and D is the diameter of the outlet nozzle.

The fabricated ram extruder was mounted on an electro-mechanic press machine. The piston of the ram extruder was connected to a load cell to record the extrusion force. Before each test, the piston ring was lightly lubricated using grease oil and driven into an empty barrel to record the friction. The friction values were kept at a bare minimum and were used as an indication of perfect barrel mounting. The barrel was filled with the prepared mix in three different layers for the tests, tampering each layer 25 times as in a previous study [25]. This was done to minimize air void and achieve maximum filling of the barrel. Selected mixtures were tested at various ages such as 20, 40, 60, 90, 120, and 150 minutes. In the present study, time counting starts by the time water comes in contact with cement (t=0.). Hence, the 20th minute, for example, refers to the time elapsed from the addition of water, the mixing procedure, and mixture placement into the barrel. It is worth noting that the 20th minute corresponds to the shortest possible period for prepared mixtures to be tested after initial operations such as mixing, barrel filling, and compaction.

2.2.4.2. Extrusion at constant material age with varying extrusion speed. To evaluate the effect of different piston moving velocities and their corresponding material flow rates on the extrudability of 3D printable mortars, the same ram extruder device described in the previous section was used. Additionally, a similar test procedure was employed. However, in this part, all mixtures were tested at the 20th minute. Here, the 20th minute indicates the shortest period at which the prepared nixes could be tested after mixing and mixture filling into the barrel. Additionally, a sharp-end orifice (12.8 mm) instead of the long die nozzle was utilized (Fig. 5). Decreasing the nozzle length is expected to reduce the friction between the material and the nozzle walls. Three different piston-moving velocities, 0.25, 1, and 1.5 mm/s, were used during the extrusion of developed mixtures.

The material flow rate (V) at the orifice was calculated using Eq. 2. Accordingly, Table 3 presents various piston movement velocities and their corresponding material flow rate at the orifice. The extrusion

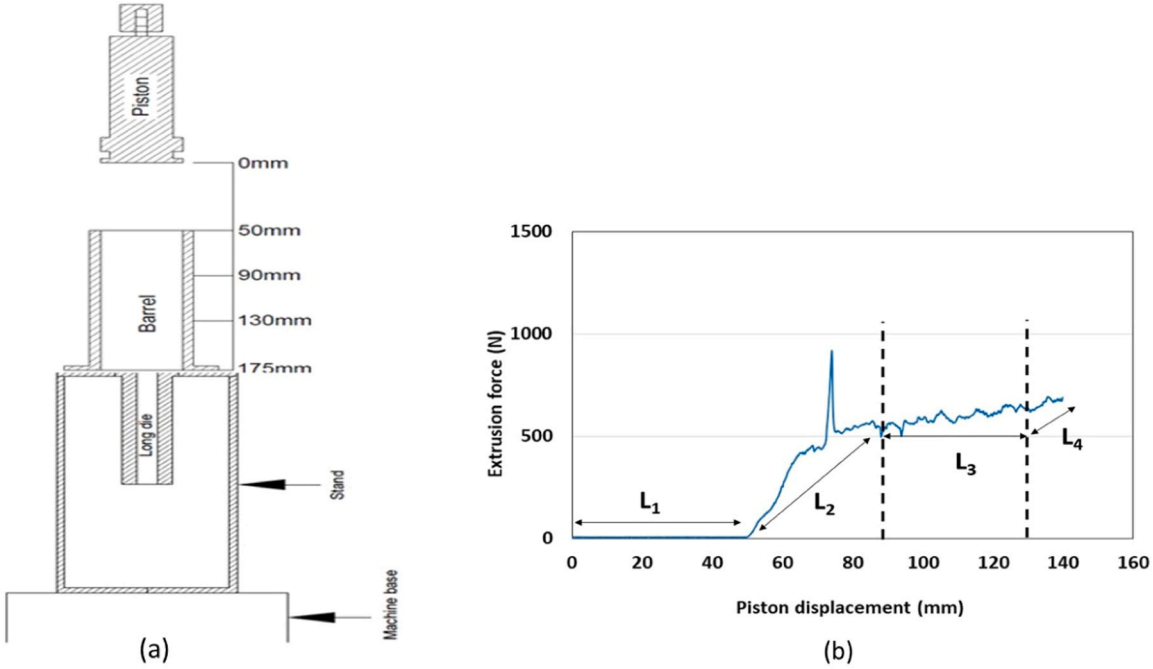

Fig. 4. Displacement zones according to the measurement protocol used for extrusion experiments (a), reflection of the resulting zones in the result (b).

Table 2
Part details of the ram extruder.

Parts name	Diameter (mm)	Length (mm)
Piston	37.4	100.0
Barrel	38.4	125.0
Long die	12.8	102.4
Short die	12.8	12.8

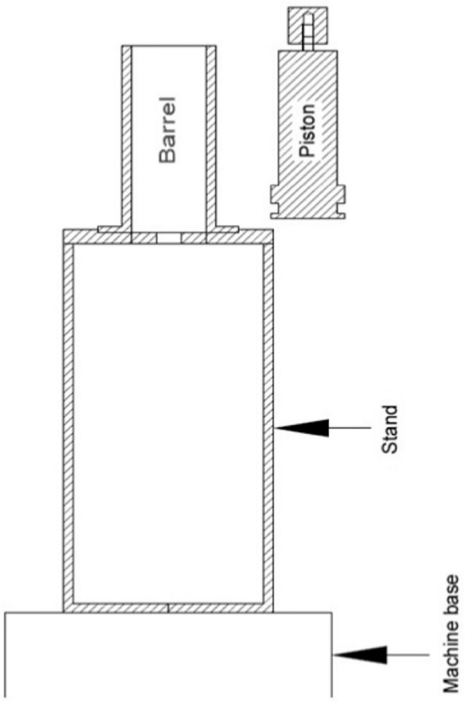

Fig. 5. Schematic section drawing of the ram extruder with a sharp-end orifice.

Table 3
Piston movement speed and material flow rate at the orifice.

V_O (Piston movement speed mm/s)	V (material flow rate in the orifice mm/s)
0.25	2.25
1.00	9.00
1.50	13.50

pressure for each flow rate was calculated using Eq. 3 in conformity with previous studies [26]. To investigate the analytical relationship between the extrusion pressure at the orifice and the material flow rate, the Basterfield model (Eq. 4) was used [24]. The analytical model was applied to the experimental data using the nonlinear least squares method and regression analysis in MATLAB. Accordingly, different material flow parameters, such as uniaxial yield stress (σo), elongational yield stress (k), and flow index (n), were determined by minimizing the root-mean-square (RMS) error. In the analytical model, a 45-degree angle, as recommended in the literature, was used for Θ_{max} [23]. Basterfield et al. [24] and Perrot et al. [27] have determined that cementitious materials can be considered to comply with the Von-Mises criterion. Therefore, the analytical relationship between the elongation-yield stress (σ_o) and shear-yield stress (τ_o) is as described in Eq. 5.

$$V = \frac{D_O^2}{D^2} V_o \tag{2}$$

In Equation 2, V_o is the piston movement velocity (mm/s), V is the material flow rate in the orifice (short die) (mm/s), D_o is the diameter of the barrel, and D is the inner diameter of the nozzle.

$$P = \frac{4F}{\pi D_0^2} \tag{3}$$

$$P = 2\sigma_o \ln\frac{D_O}{D} + \frac{2}{3n} k(\sin\Theta_{max}(1+\cos\Theta_{max}))^n \left(1 - \left(\frac{D}{D_O}\right)\right)^{3n} \left(\frac{2V}{D}\right)^n \tag{4}$$

Where P is the extrusion pressure, F is the average extrusion force recorded during extrusion, and D_o is the inner diameter of the barrel.

$$\tau_0 = \frac{\sigma_o}{\sqrt{3}} \quad (5)$$

In Eq. 5, σ_o represents the elongational yield stress, and τ_o represents the shear yield stress.

2.2.5. Rheological measurements with vane type measuring cell

Understanding and controlling the rheological properties of the concrete mix is essential to achieve successful and precise deposition layer-by-layer while ensuring structural integrity and quality of the printed components. Accordingly, to determine the effect of HPMC and its dosage on the rheological properties of mixtures formulated with different binder and aggregate volumes, a rotational rheometer (Anton Paar Physica MCR 51 rheometer, ST59–2V-44.3/120 striper) was employed. The Vane system was chosen to minimize the wall slip effect. The vane system is also suitable for measuring the relative rheological properties of granular suspensions (i.e., cement mortar). During the test, all mixes were tested at ambient temperature (22 °C). For this method, firstly, a constant shear rate of 0.1 s^{-1} was applied for 120 s, as shown in Fig. 6-a. During this process, as the sample is not disrupted, the static yield stress has been obtained from the peak value in the measurements. Then, each mixture was subjected to shearing force with a linearly increasing shear rate from 0 s^{-1} to 0.1 s^{-1} in 15 s, providing a more homogenous and stable condition for reliable measurement during Bingham modeling. Afterward, 5 s resting time was followed, and in the last step, shear load with a linearly decreasing shear rate from 0.1 s^{-1} to 0 s^{-1} within 15 s was applied to each mixture, as shown in Fig. 6-b. The plastic viscosity and dynamic yield stress are obtained by fitting the down-curve with the Bingham model (Fig. 6- b, Stage III), and the calculation range is in the stabilization stage of 20 s to 35 s. The differential area between ascending and descending flow curves has been calculated and called the hysteresis area [28]. The hysteresis area values have been associated with the structural recovery potential of mixtures.

Unlike previous studies, Ilcan et al. [29] and Panda et al. [30], two different macros were used in assessing static yield stress and flow curves. The macros individually used for static yield stress and flow curves are schematically presented in Fig. 6. When measuring static yield stress and determining the flow curves in a single sample, the initial measurement at 15 minutes represents the undisturbed state of the sample, while subsequent measurements at later ages represent the disturbed state (with a vane probe previously inserted to create a trace). Additionally, it is believed that the mixing process in the static yield stress region may affect the flow curves when static yield stress measurements at a constant deformation rate are compared to flow curves obtained at decreasing and increasing rates within the same sample (on a single macro scale). Therefore, tests were conducted on two different samples, the initial sample for static yield stress and the re-prepared sample for flow curves, to obtain relevant parameters from undisturbed samples. These macros allow the measurements of static yield stress and dynamic yield stress to be performed separately on undisturbed samples. Two different measurement times for static yield stress were chosen: 15 minutes and 30 minutes. Within this measurement protocol, mixtures with cement dosages of 850, 900, and 950 kg/m^3 were tested at three different HPMC dosages.

2.2.6. Green strength

Green strength tests were performed to study the buildability of the selected mixtures in their fresh state. For this, cylindrical molds with 60 mm in height and 30 mm inner diameter (Fig. 7) were prepared using flex glasses. It has been reported that during uniaxial compression tests, the formation of a diagonal shear failure can be assured by using samples with a slenderness (h/d) of 2 [31]. Green strength tests were performed using displacement control at a rate of 0.20 mm/s, as in the study by Chen et al. [32]. It is worth noting that samples were loaded to a 40 % longitudinal deformation. A load cell of 6 kN was used to record the resulting loads. In addition, as in the studies [32,33], to calculate the lateral deformation of the samples, a Cannon PowerShot S5 IS camera was set to automatically capture images at an interval of an image every 5 seconds. Captured images were then processed using image processing techniques in MATLAB program. Processed binary images were employed to calculate lateral and vertical deformation with the help of a MATLAB code. The stress values created by the loads measured after the test in the deformed samples were determined by dividing the load by the enlarged cross-sectional area formed during loading. Lateral and vertical deformation were determined and calculated with the help of a MATLAB code. Care was taken to ensure that the positioning of the camera remained the same throughout the experiments.

After mixing, fresh mixtures were filled into prepared plastic molds in 3 layers by carefully tamping each layer 25 times. The molds were then covered with a plastic film and stored at ambient temperature in an air conditioning cabinet at 20 ±2 °C and 50 % relative humidity (RH) until testing time. At least three samples were demoulded and tested at

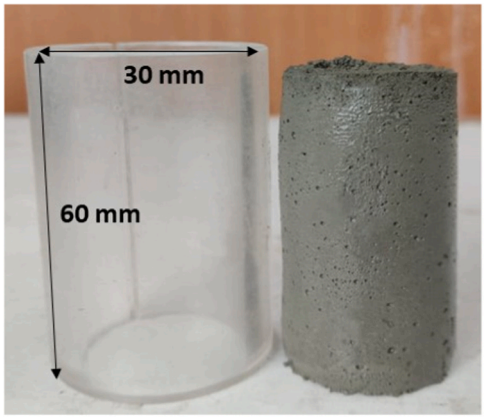

Fig. 7. Cylindrical specimen mold and dimensions prepared for green strength test.

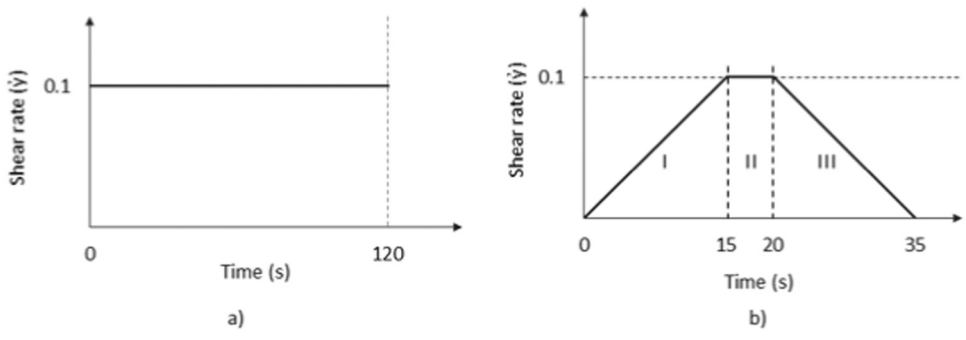

Fig. 6. Static yield stress (a), yield curves, and dynamic yield stress (b) measurement macro.

each material age, i.e., 20, 40, 60, 90, 120, and 150 min. Two layers of plastic sheets were used at both ends of the sample during testing to alleviate friction between the sample and the machine base plates.

2.2.7. Mechanical properties

Flexural strength tests were performed on molded specimens at 7 and 28 days of standard water curing. The tests were carried out using a three-point bending test according to TS EN 196–1. A displacement-controlled electromechanical test device with a capacity of 100 kN was used. A loading speed of 2.4 kN/s was used during the tests. At least three prismatic mold samples with dimensions of 40×40×160 mm were used. A span of 130 mm was used between the two supports.

Compressive strength tests were conducted on molded specimens in accordance with TS EN 196–1. The compressive strengths of at least three specimens with dimensions of 40×40×40 mm were determined after 7 and 28 days of standard water curing. A hydraulic pressure press with a capacity of 3000 kN was used. The loading rate was kept at 2.4 kN/s during the experiments.

3. Results and discussion

3.1. 3D printable mixtures development

Flow diameters of 3D printable mixtures developed in the present study are presented in Table 4. The developed mixtures were produced with various cement dosages, namely 850, 900, and 950 kg/m^3, corresponding to various aggregate volumes of 44 %, 41 %, and 38 % and at a constant water-to-binder (W/C) ratio of 0.3. The W/C ratio was selected as it is widely used in the literature [6]. The HRWRA dosage was adjusted for each cement dosage to achieve a target constant flow value. These target flow values were 290±10 mm, 180±10 mm, and 150 ±10 mm for mortars without HPMC and those with an HPMC dosage of 0.14 % and 0.28 % by weight of cement, respectively. It is worth noting that, unlike the flow diameters of HPMC-containing mixtures measured after 25 drops of the flow table, those of HPMC-free mixtures were self-flow. It is seen that the required HRWRA dosage to achieve a given flow value decreases with increasing binder volume. Since the increase in binder volume is synonymous with a decrease in aggregate volume. It can also be said that the dosage of HRWRA required for a certain flow diameter increases proportionately to the volume of aggregate in the mix. The increase in HRWRA demand with an increase in aggregate volume can be attributed to the rise in interparticle friction as the aggregate volume increases [34].

Furthermore, it has been observed that the flow diameter of these mixtures is directly proportional to the HPMC dosage contained in their formulation (Fig. 8). Regardless of the cement dosage, the flow diameter of all mixtures decreased with an increase in HPMC dosage, as expected. It has been determined that an HPMC of 0.14 % and 0.28 % yielded flow diameters of 180 ±10 mm and 150±10 mm, respectively. The cohesion-improving effect of HPMC, which can be attributed to its entangled polymer structure, imbibes significant amounts of mixing water, leading to a viscosity increment [35].

Mixtures with the aforementioned flow diameters were tested to assess their printability and buildability with the help of a manual injection gun. The obtained results are presented in Fig. 9. It has been found that the buildability of these mixtures is proportional to their flow diameters. It was observed that mixtures with higher flow diameters exhibited poor buildability and vice versa. In contrast to buildability, it has been observed that the shape stability of these composites ranges within a threshold value or range that should not be exceeded (or surpassed) (140–190 mm). Printed filaments exhibit a wider width when the flow diameter exceeds this range. On the contrary, when the flow diameter is below this range, they become thinner (smaller width) or exhibit width non-uniformity. It is worth noting that since the extrudability is assessed by the ability of a mix to be continuously extruded through the nozzle without blockage and discontinuities, a higher flow diameter favors the extrudability while negatively affecting the shape stability and buildability. Accordingly, it has been noticed that stiff mixtures, which is a synonym for mixtures with low flow diameters, led to failure during printing by either cracking of the filament or nozzle clogging due to the stiffness of the mix. On the contrary, very high flow diameters led to very poor shape stability. In conclusion, it has been determined that a flow diameter ranging between 140 and 180 mm yielded the best shape retention, printability, and satisfactory buildability.

In Table 4, a higher binder content, which is characteristic of printable mixtures, can be observed [36]. In their review of the performance requirements of printable mixtures, Hou et al. (2021) concluded that a higher binder volume is necessary to enhance the thixotropy of these mixtures [37]. Consequently, a higher binder content is known to be inducive to autogenous shrinkage. Additionally, the non-utilization of formwork leads to higher plastic and drying shrinkage of these mixtures [38–40]. Kheir et al. (2021) reported an increase in shrinkage strain with a decrease in the s/b ratio, which can be associated with a reduction in the restraining effect of the aggregate with a decrease in the s/b ratio [38]. It is worth noting that autogenous shrinkage is prevalent in cementitious mixtures with a higher binder content and a w/c ratio lower than 0.42 [38]. The increase in shrinkage deformation with a decrease in the s/b ratio is related to the self-desiccation effect of cementitious materials in that their volume decreases after hydration, leading to internal stresses that result in shrinkage cracks.

3.2. Setting times

Table 5 presents the initial and final setting times of the developed 3D printable mixtures. The findings of the present study indicate that the addition of HPMC slightly affected the setting times of developed mixtures. It has been observed that there exists a directly proportional relationship between HPMC dosage and the setting times of these mixtures. Furthermore, while the addition of HPMC slightly lengthened the initial setting times of all the mixtures, it slightly reduced their final setting times except for the mixture with 950 kg/m^3 cement dosage, of which the setting times slightly increased. An interesting finding is that

Table 4
Design of printable mixture and flow diameters.

Mixture Codes	Cement kg/m^3	Sand kg/m^3	Water kg/m^3	HRWRA kg/m^3	HPMC kg/m^3	HPMC %	Aggregate Volume %	Flow Diameter mm
850 H0	850	1097	256	8.1	0.0	0	44	305
850 H0.14		1094	256	8.1	1.20	0.14	44	170
850 H0.28		1092	256	8.1	2.41	0.28	44	149
900 H0	900	1021	272	5.9	0.0	0	41	280
900 H0.14		1019	272	5.9	1.27	0.14	41	178
900 H0.28		1017	272	5.9	2.55	0.28	41	143
950 H0	950	944	288	5.2	0,0	0	38	282
950 H0.14		941	288	5.2	1.35	0.14	38	183
950 H0.28		939	288	5.2	2.69	0.28	38	145

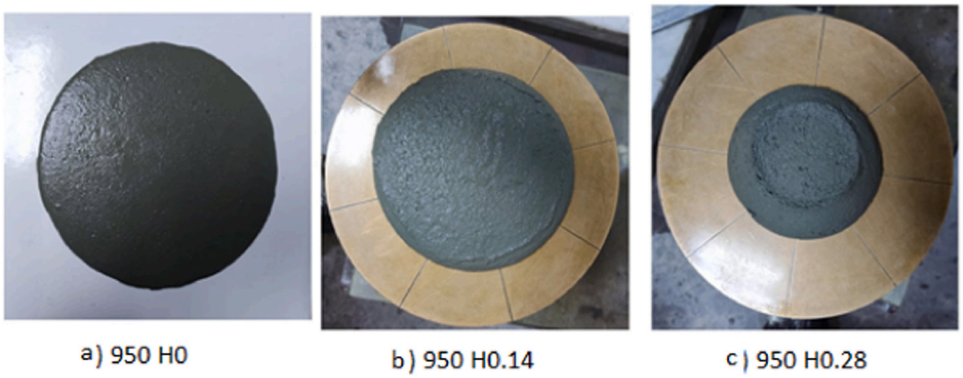

Fig. 8. Flow diameters of 950 H0, H0.14, and H0.28 mixtures.

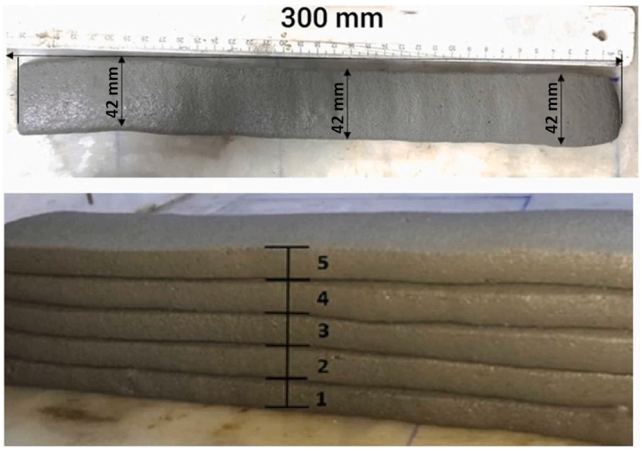

Fig. 9. Shape stability (top) and buildability tests with manual injection gun (bottom).

Table 5
Setting times of mixtures containing HPMC.

Mixture Type	Initial setting time (min)	Final setting time (min)
850 H0	205	255
850 H0.14	210	220
850 H0.28	225	235
900 H0	220	275
900 H0.14	235	250
900 H0.28	240	255
950 H0	195	225
950 H0.14	220	230
950 H0.28	225	235

while HPMC addition retarded the initial times, it led to a quick stiffening right after the initial setting by accelerating the final setting. This can be seen by considering the period between the initial and final setting times in the presence of HPMC. The shortest period in HPMC-free mixtures was 30 minutes, recorded from mix 950 H0. In the presence of HPMC, the longest time span decreased to 15 minutes, recorded from mix 900 H0.14. These findings are similar to previous studies that reported that HPMC shortened the time interval between the initial and final setting times [5]. It can be inferred that HPMC extends the dormant period by elongating the initial setting time during which the mix retains its plasticity and remains sufficiently workable. Unlike nanomaterials such as silica fume, it can be inferred that HPMC provides an extended printability window, a significant advantage in 3D printing processes. The increase in the induction period in the presence of HPMC is due to the long-chain polymers of HPMC adsorbing onto cement particles, which retards the absorption rate of H_3O^+ ions for further reaction [41, 42].

3.3. Extrusion test

3.3.1. Extrusion at varying material age with constant extrusion speed

A graph displaying the piston displacement-extrusion forces curve recorded during the extrusion of 3D printable mixtures of the present study at various ages is presented in Fig. 10. As per the test protocol, recorded graphs illustrate the presence of four different zones. In the first zone (0–50 mm), where the piston moves freely before reaching the level of the barrel, the recorded extrusion force is at the lowest level, and no force is recorded. In the second zone (50–90 mm), the contact between the piston and mixture in the barrel is initiated. This zone is characterized by a sharp and steady increase in extrusion force. This exponential increase in extrusion force at this zone can be attributed to the compaction of the material in the barrel before material extrusion through the nozzle starts.

Right after mixing, cement particles at rest start to flocculate under the influence of colloidal attractive forces, resulting in a network able to resist any flow initiated by stresses lower than this inherent threshold stress known as yield stress [43]. As a result of flocculation, nucleation takes place at the pseudo-contact points within the flocculated network, turning the weak colloidal network into strong interactions that may be regarded as solid bridges. With the formation of these solid bridges, a further increase in elastic modulus occurs. Within a few progressive seconds, a percolation path of cement particles intertwined solely through hydrate bridges, commonly known as structuration, can be observed at the macroscopic scale. Additionally, it is worth noting that at a macroscopic scale, non-reversible chemical bonds lead to the formation of hydrate bonds between particles at this stage. It has been demonstrated that these bonds can be broken by shearing or remixing forces and can reform at rest, given the availability of enough chemical compounds for their interaction. Hence, the sharp increase in extrusion forces recorded at this zone may be associated with the breaking of these hydrate bridges, which are at the origin of structuration [9]. It is worth remembering that the successful development of 3DPC mixtures relies on the utilization of flocculants or nanomaterials that accelerate or increase structuration either physically by increasing the number of available nucleation sites or by accelerating chemical reactions. It has been observed that as the time at rest increases, the extrusion forces at this stage also increase. This can be attributed to the formation of stronger hydrate bridges with time. At the end of the compaction zone, extrusion forces reach a steady state, and the material extruded at the nozzle flows steadily. As determined by Perrot et al. [44], the extrusion pressure required for the extrusion should be correlated with extrusion forces at this stage. Finally, as the piston nears the end of the barrel, a non-linear increase in extrusion force is observed due to the existence of the dead zone, leading to a non-uniform flow of the material. The curves

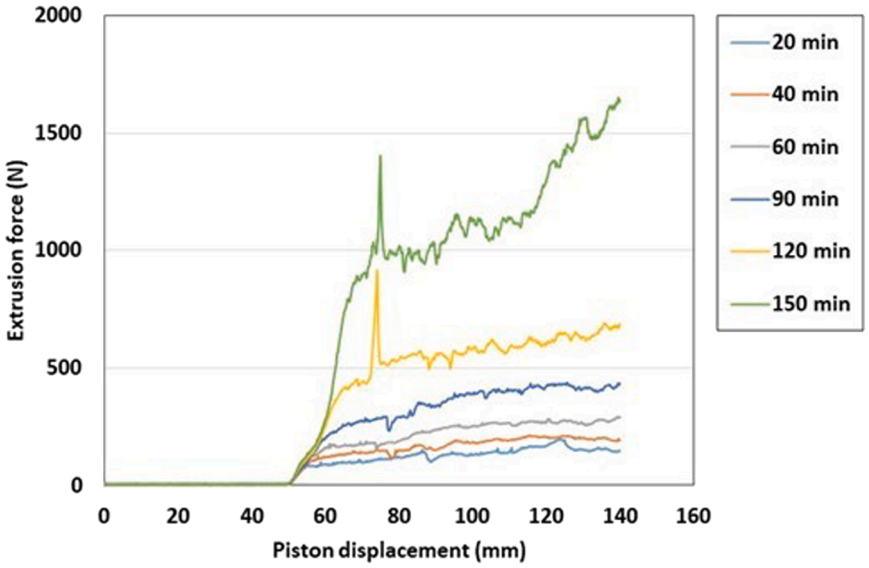

Fig. 10. Typical piston displacement-extrusion force graph (taken from mix 900 H0.14).

obtained as a result of experiments in the present study are similar to those reported in previous studies [9,45].

Previous studies have shown that improper mortar designs led to the drainage of water from granular materials during extrusion disrupting the integrity of the mixture and resulting in very high extrusion forces [26]. This phenomenon has been associated with high aggregate volume and insufficient dosages of HPMC. Similarly, reference mixtures without HPMC were observed to flow under their own weight after being placed in the barrel. In other words, such mixtures lack sufficient shape stability at early ages, such as 20, 40, and 60 minutes, and can thus not be considered 3D printable. Furthermore, the extrusion of these mixtures at later ages, starting from 90 minutes, led to segregation and flow blockage (Fig. 11).

The extrusion pressure results of the developed mixtures are presented in Fig. 12, whereas Fig. 13 presents images of mixtures after extrusion. Since all the reference mixtures (850 / 900 / 950 H0) were in a fluid consistency at early ages (20, 40, and 60 minutes) and decomposed after 90 minutes, they could not be extruded at any measurement age. The findings of this study show that HPMC improved the extrudability of all mixtures, especially at early ages. It is also seen that the addition of HPMC prevented mixtures from segregating at advanced ages, such as 90, 120, and 150 minutes, and made them extrudable even at these ages. As shown in Fig. 12, the extrusion force is directly proportional to the material age for all mixtures, regardless of the mixture composition. In other words, the extrusion force increases as the extrusion age increases. This result can be attributed to the increase in structuration due to HPMC addition. The increase in the structuration of cement-based mixtures is synonymous with the rise in static yield stress [46]. In addition, it was observed that an increase in HPMC dosage caused a slight increase in the extrusion forces of all mixtures at 20 minutes of material age. However, this trend changed after the 40th minute, except for mixtures with a cement dosage of 850 kg/m^3 where higher extrusion force is required to extrude mixtures with low HPMC content. As shown in Fig. 12, the extruded mixtures exhibited excellent shape stability, especially at early ages. Moreover, the shape of the extruded materials improved with age for all mixtures up to the 60th minute. It has been observed that from the 90th minute, mixtures with low HPMC dosages lost their rigidity by torsion and cracking while being extruded. Accordingly, a higher extrusion force was required for the extrusion of these mixtures (Fig. 12). In contrast, relatively lower extrusion forces were recorded during the extrusion of mixtures with higher HPMC dosage at later ages. In harmony with this, these mixtures did not exhibit any cracking even at later ages (Fig. 13). This further confirms the set retarding effect of HPMC as previously noted in setting times results. It can be understood that as the HPMC dosage increases, the time interval in which mixtures remain printable increases as well. In other words, HPMC extends the printability window of these mixtures. In addition, it was noticed that the extrusion forces of mixtures with low HPMC dosage did not reach a steady state in the measuring zone at the 150th minute. This can be attributed to the formation of hydrate products due to the chemical reaction between cement and water, known as hydration. Furthermore, it was determined that at early ages (from 20 to 40 min), the effect of increasing HPMC dosage on the extrusion force concerning different aggregate volumes was negligible. However, at later ages (from 60 minutes), it was seen that higher HPMC dosage had a more accentuated effect on mixtures with higher paste volumes (lower aggregate volume) in such that it kept their extrusion forces lower, preserving their extrudability. Hence, it can be concluded that the effect of HPMC dosage on the extrudability is more pronounced at later ages for mixtures with higher paste volumes.

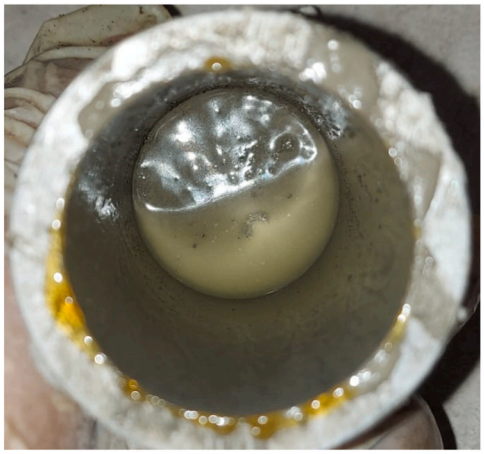

Fig. 11. Drainage of water from the mix for HPMC-free mixtures during extrusion.

3.3.2. *Extrusion at constant material age with varying extrusion speed*

Fig. 14 presents an example of piston displacement-extrusion force curves measured at constant material ages (t=20 min). As in the

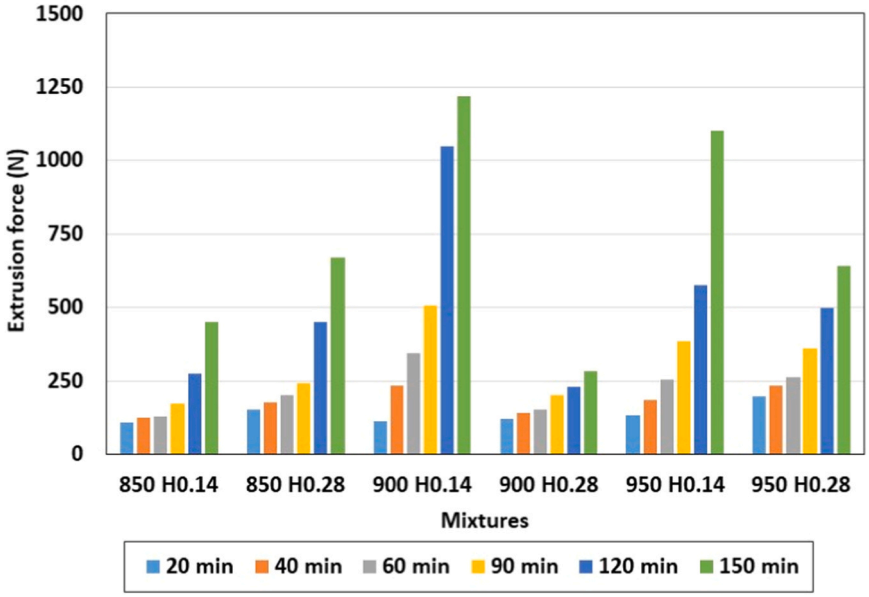

Fig. 12. Extrusion forces of various mixtures at different mortar ages.

previous measurements, the average extrusion force was calculated in the region where the extrusion forces reached a steady state (90–130 mm). Fig. 15 presents recorded extrusion forces for each piston velocity and mixture comparatively. Additionally, the effect of nozzle length on the extrusion forces of developed mixtures is shown in Fig. 16. Table 6 shows the material flow parameters obtained by correlating the experimental results with the Basterfield model.

Basterfield et al. [24] and Nerella et al. [47] showed that the piston movement speed is directly proportional to the material flow rate at the orifice. Similarly, the extrusion pressure is proportional to the extrusion force. The results of this study show that both extrusion pressure and extrusion force increased with increasing piston moving velocity, regardless of mix composition.

It was observed that at equal piston moving velocity, an increase in HPMC dosage resulted in an increase in extrusion force for all mixtures. Furthermore, the highest extrusion forces at all studied piston moving velocities were recorded from 850 kg/m^3 cement dosage mixtures, corresponding to the highest aggregate volume. Mixtures with 900 and 950 kg/m^3 cement dosages showed very close extrusion forces. It can be inferred that a high volume of aggregate can lead to higher extrusion forces, adversely affecting the extrudability of these mixtures. The increase in extrusion forces with increasing aggregate volume can be attributed to the increase in particle friction. When the experimental results of all mixtures were modeled with the Basterfield model, the R^2 values obtained were quite high (Table 6). Therefore, it can be said that the mixtures developed in this study appear to be compatible with the Basterfield analytical model. As can be seen from Table 6, the increase in HPMC dosage led to an increase in k, n, σ_o, and $\tau_o$values in all mixtures except for the 850 H0.28 mixture. It is worth understanding that the increase in static yield flow stress (σ_o), flow consistency "k", and shear yield stress (τ_o) indicate that HPMC addition led to the reduction of flowability of these mixtures. In practice, this is beneficial for shape retention and buildability. Similar results on the increase in these flow parameters with the increase in HPMC dosage have been previously reported in the literature [10]. From these results, it can be deduced that the addition of HPMC significantly increases the extrudability of 3D printable mixtures, especially at an early age. Flow parameters determined from the 850 H0.28 mixture are inconsistent with those of the other mixtures. This is believed to be due to the combination of high aggregate volume and HPMC dosage. Hence, the negative values obtained as a result of fitting the experimental results to the Basterfield model have been assumed to be zero.

In previous studies, researchers reported that an increase in extrusion speed during ram extrusion could result in an increase in extrusion force. This situation can be attributed to three main factors: 1. Shear forces: As the piston movement speed increases, the mixture encounters higher shear forces, and the particles in the mixture move towards each other. This causes an increase in flow resistance and leads to an increase in extrusion force. Jayathilakage et al. [48] observed that the increase in piston speed increases the shear forces and causes an increase in the extrusion force. 2. Friction: At higher speeds, a more frictional force is created between the surface of the extruder and the mix. This increases the force required for the mixture to pass through the extruder and nozzle. Lu and Wang [49] found that the friction forces between the mixture and the extruder surfaces increase with increasing piston speed, increasing extrusion force. 3. Deformation: The mortar mix is a non-Newtonian fluid whose viscosity changes depending on the deformation rate. At higher speeds, the mixture deforms faster, resulting in higher viscosity and a higher resistance to flow. In this case, it causes an increase in extrusion force. Perrot et al. [50] observed that an increase in piston speed increases the deformation of the mixture, resulting in higher viscosity and an increase in extrusion force.

In this study, when the extrusion forces required for the extrusion of mortar mixtures are examined at equal age (t=20 min) and piston movement speed (1 mm/s), it is seen that the extrusion forces increase as the length of the nozzle increases. As shown in Fig. 16, extrusion forces are higher in a long spout than in a short spout. This is due to the friction effect that increases in direct proportion to the nozzle length. This result may reflect the impact of pump hose length on extrusion pressure during printing operation.

3.4. Rheological measurements

In the present study, the effect of HPMC on the rheological properties of 3D printable mixtures was investigated by measuring various rheological properties, such as static yield stress, dynamic yield stress, and plastic viscosity, which are characteristics of 3D printable mixtures. Accordingly, the aforementioned rheological properties were determined at 15 and 30 minutes. It is worth noting that undisturbed samples were utilized for each experiment. In line with this, Figs. 18 and 19 present the determined yield stress-time and flow curves of mortars for each investigated cement dosage at 15 and 30 min. In both curves in

Fig. 13. Images of different mixtures after extrusion.

Fig. 18, the red arrow indicates the ascent curves, and the blue arrow indicates the descent curves. Additionally, Table 7 presents the determined values for various investigated rheological properties: dynamic yield stress and plastic viscosity at 15 and 30 minutes.

The present study's findings show that the addition of HPMC led to an increase in static yield stress, dynamic yield stress, and plastic viscosity. Previous studies have shown that HPMC can improve the printability of paste by increasing plastic viscosity and yield stress [51–53] and by enhancing the rheological stability [54] of the paste. Additionally, it has been observed that there exists a directly proportional relationship between material age at testing and these rheological properties. Similarly, the increase in HPMC dosage led to an increase in these properties at all ages, with the exception of a mix with 950 kg/m^3 at 30 min, which exhibited a slightly different trend. Another interesting finding showed that the effect of HPMC dosage was significant at early ages. However, as material age grows, this effect decreases. It can be inferred that the rate of structuration is maximized at low HPMC dosage. This can be understood by considering the rate of static yield stress increment at 15 in comparison to 30 min. Attributable to the water retention properties of the HPMC admixture, it has the capacity to significantly retard the rate of water evaporation, thereby facilitating more thorough hydration of the cementitious material [53]. Consequently, this contributes to the formation of a robust microstructure in the mortar, resulting in an elevated static yield stress.

In contrast to previous studies in the literature, no significant trend is observed regarding the effect of binder volume on the investigated rheological properties. This can be attributed to the fact that the investigated mixtures were produced with an equal w/c ratio and tailored to possess equal workability.

It is a well-established fact that the static yield stress of cement-based mixtures increases with ages due to the formation of hydration production through the reaction of cement compound with water. However, the increase observed in the present study can only be attributed to using HPMC rather than hydration at an early age.

At an early age (15 min), fresh mortar mixtures with low HPMC dosages of 900 kg/m^3 H0.14 and 850 kg/m^3 H0.14 exhibited high static yield stress values (Fig. 17 (a)). On the other hand, at an advanced age (30 min), fresh mortar mixtures with a cement dosage of 900 kg/m^3 demonstrate the highest increase rates in static yield stress, with both HPMC dosages being close to each other (Fig. 17 (b)).

The static yield stress of concrete generally increases with time as the hydration process progresses and the concrete gains green strength. During the initial stages of hydration, concrete undergoes a rapid period of chemical reactions as water reacts with cement particles. At this stage, the static yield stress is relatively low as the cementitious matrix is still in the process of gaining strength. The concrete is more susceptible to deformation and may not be able to withstand high stresses without significant deformation. As time progresses, the hydration reactions continue, and the concrete gradually sets and hardens. The static yield stress increases as the cementitious matrix gains strength and stiffness. The development of interlocking crystals and the formation of calcium silicate hydrate (C-S-H) gel contribute to the increasing static yield stress over time.

The hysteresis areas at 15 minutes and 30 minutes for HPMC and non-HPMC mixtures at different cement dosages were calculated from the yield curve graphs given in Fig. 19, respectively. In the given graphs, the arms showing high shear stresses indicate the last stage in the macro as the descending curve. The cases where the yield curve is below the descending curve indicate negative hysteresis areas. Materials exhibiting high structural recovery behave as rigid at rest but become fluid when force is applied. Table 7 and Fig. 19 show the hysteresis areas of the mixtures. All mixtures showed a negative hysteresis area, i.e., structural recovery behavior [28]. It is seen that the hysteresis areas of the mixtures without HPMC are low at all cement dosages, and the hysteresis areas increase with the addition of HPMC to the mixtures. Especially the 900 kg/m^3 H0.14 mix was the mix that showed fast recovery at both ages. According to the study by Chen et al. [10], viscosity modifiers change the rheology of concrete by improving the thixotropic properties. Thus, the viscosity of concrete decreases when the force is applied, providing easy handling and good pumping, and the viscosity increases when the force is removed so that the mortar mix exhibits better shear resistance at rest. It is also observed that the hysteresis areas

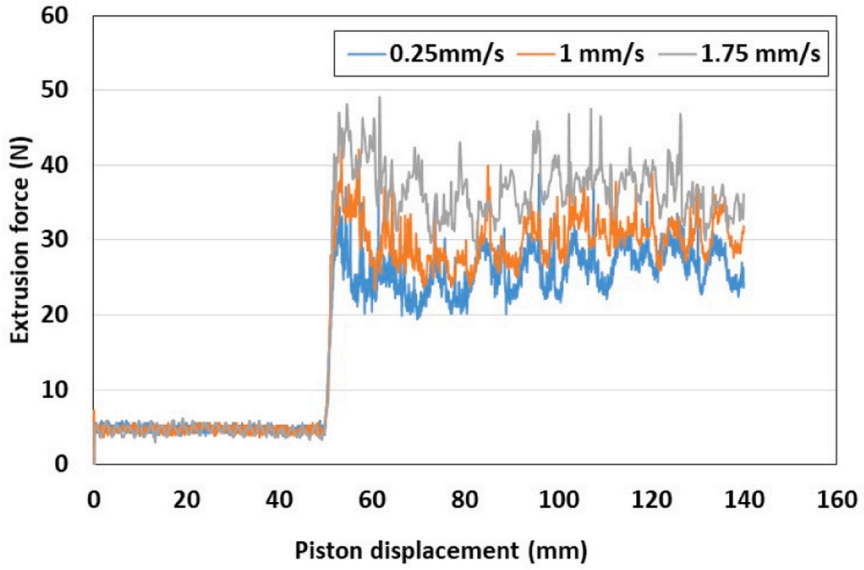

Fig. 14. The piston displacement-extrusion force curves measured at constant material ages (t=20 min).

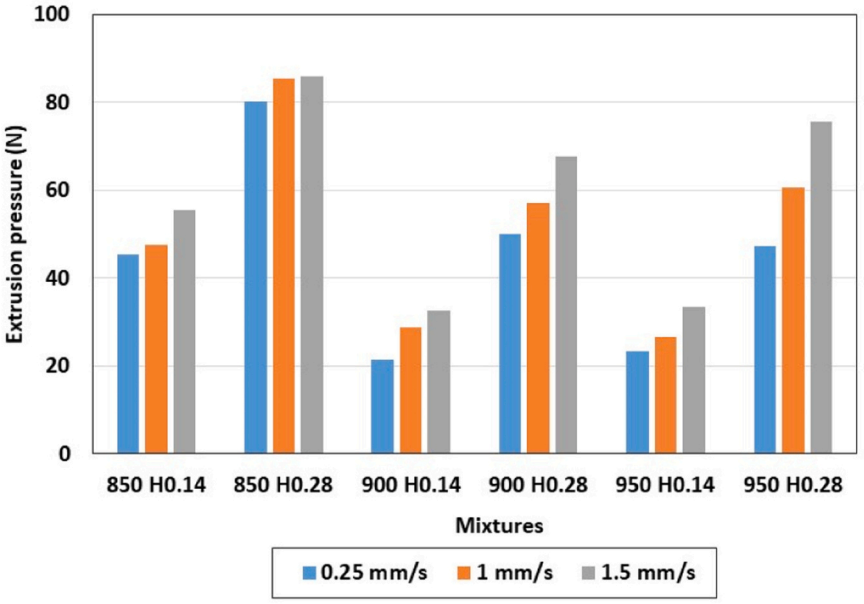

Fig. 15. Extrusion forces comparison for each piston speed and mixture.

increase as the age of the fresh mortar increases.

Table 7 and Fig. 20 present the development of dynamic flow curves of the mixtures at t = 15 and 30 minutes, depending on the HPMC dosage. The dynamic flow curves of all mixtures tended to shift upward with the addition of HPMC. When a low dosage of HPMC was added, the 900 kg/m^3 H0.14 mixture showed the highest dynamic flow curve values, while with a high dosage of HPMC, the 900 kg/m^3 and 950 kg/m^3 H0.28 mixtures exhibited the highest values. Among the mixtures containing HPMC, it was observed that the mixtures with lower HPMC dosages (850 kg/m^3 H0.14 / 900 kg/m^3 H0.14 / 950 kg/m^3 H0.14) had lower plastic viscosity values. Plastic viscosity decrement due to shear positively affects the mortar rheology at the pumping and extrusion stages [9].

A similar trend was observed when analyzing the hysteresis areas graph in Fig. 19. Mixtures with higher HPMC dosages exhibited larger hysteresis areas. Fig. 21 shows the development of the mixtures' viscosities based on the HPMC dosage and time. The viscosity of all mixtures increased over time, and the same trend was observed with an increase in HPMC dosage. This is an expected result due to the viscosity-enhancing property of HPMC additives.

The static yield stress values measured at 15 and 30 minutes for the mixtures are given in Table 7. Fig. 22 presents a comparative graph of the development of static yield stress values over time for the mixtures. As a general trend, the static yield stress value increases as the fresh mortar age increases, as expected. An increase in HPMC dosage significantly increases the static yield stress values, especially in the first 15 minutes. This is because the addition of HPMC slows down the evaporation rate of water due to its water-retention properties, allowing for more complete hydration of the cementitious material. This contributes to the development of a more robust microstructure in the mortar, leading to higher static yield stresses. However, increasing the HPMC dosage to the level of 0.28 % in the 30 minutes, when the fresh mortar age has increased, did not provide the same contribution to the static yield stress. When the fresh mortar age increased from 15 minutes

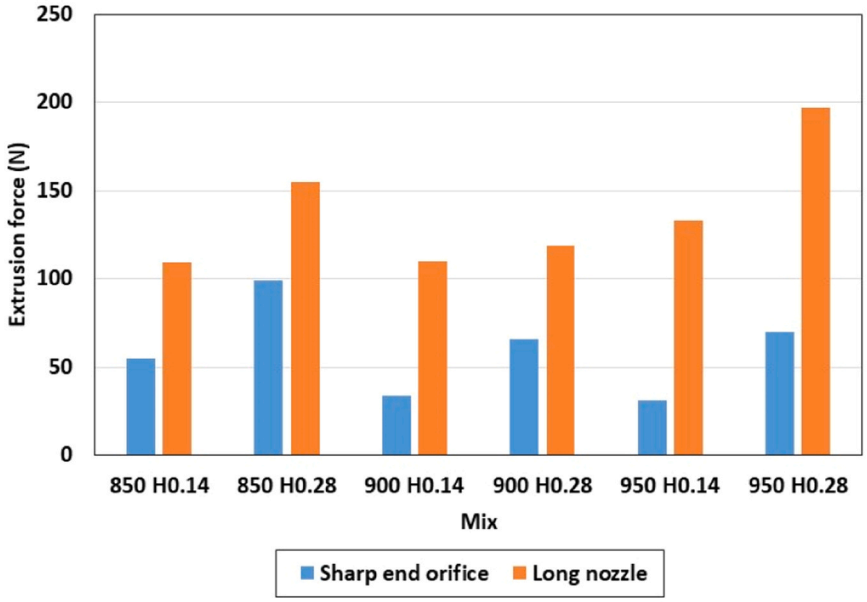

Fig. 16. The effect of nozzle length on the extrusion forces of developed mixtures (piston movement speed 1 mm/s).

to 30 minutes, the static yield stress value of HPMC-containing mixtures increased by a minimum of 1.3 to a maximum of 5.9 times. As shown in Fig. 22, in mixtures without HPMC, the static shear strength increases as the aggregate volume decreases (and cement dosage increases), rising within the first 15 minutes and showing an increase, though not linear, at 30 minutes. It was determined that at an early age (15 min), the contribution of HPMC dosage on static yield stress was weakened in the case of higher paste volume. In other words, the addition of HPMC results in a pronounced increase in the static yield stress at a lower paste volume. Furthermore, the increase in static yield stress with HPMC is not linear. In comparison to the HPMC-free mixture, the addition of 0,14 % HPMC by binder weight increased the static yield stress by 18, 11, and 5 times, whereas doubling this dosage led to 40, 17, and 8 times increase in static yield stress for mixtures 850, 900, and 950 kg/m^3 respectively. Moreover, it was observed that the effect of HPMC dosage on the growth rate of static yield stress with time is almost identical regardless of the aggregate volume.

The structural build-up of concrete is affected by the volume and characteristics of aggregates [9]. Ivanova and Mechtcherine pose a hypothesis that there might exist physical-chemical interactions between fine aggregates [55] and cement paste. The static rheological properties of concrete can be significantly affected by variations in the volume fraction of aggregates and thereafter fine-tuned by changing the surface area of aggregates or, in other words, by modifying the particle size distribution. Static yield stress defines the constructability in terms of shape stability after extrusion [9]. Both HPMC-containing and non-containing mixtures show that the best mixture in terms of static yield stress is the one with a cement dosage of 900 kg/m^3.

3.5. Green strength

Green strength tests were carried out on prepared samples at various early mortar ages such as 20, 40, 60, 90, 120, and 150 min. Applied strains reached up to 40 %, equivalent to 24 mm vertical displacement in a displacement-controlled compression test. The green strength of printable concrete is analogous to the maximum reachable height without collapsing during printing [26]. The load-displacement curves as a result of performed experiments are presented in Fig. 23. Using the recorded load and the continuously captured strains during loading, stress-strain curves were calculated using a MATLAB code as in previous studies. The calculated stress-strain curves are presented in Fig. 24. In these graphs, the light dashed lines correspond to the load-displacement / stress-strain curves of each sample at every testing age. Meanwhile, the dark solid-dashed lines show the average curve of the three samples. Furthermore, in Fig. 25, the time-dependent developments of green strengths of all mixtures are given.

Since green strength tests were carried out on fresh samples, it is worth mentioning that tested samples were sorted based on their shape stability right after demolding. Accordingly, vertical deformation of up to 20 % led to the disqualification of the sample in question. As a result, samples prepared from reference mixtures (i.e., 850 H0, 900 H0, and 950 H0) exhibited poor shape stability up to 120 min when they became stable, as can be seen in Fig. 26.

In Fig. 23, it can be seen that, in general, the recorded load-displacement curves exhibit a directly proportional trend between the load and the displacement. In other words, as the displacement increases, the load also increases. When the calculated stress-strain curves in Fig. 24 are observed, it is apparent that two distinct trends exist in the curves. In the first trend, the stress increases linearly with strain up to a certain plateau, which remains constant regardless of the stress. In the second trend, the stress increases linearly with strain up to the maximum point from which it decreases as the strain increases. Hence, the plateau in the first trend and peak stress in the second are considered the maximum load and stress of samples, respectively.

Regardless of mix composition, the green stress increases with material age in all mixtures. The increase in strength with time for cementitious composites is a well-known and understood phenomenon. In general, cementitious composites gain strength with time through the hydration of cement compounds with water. The addition of HPMC significantly improved the green strength of all mixtures, especially at early ages. This can be explained by the ability of HPMC-contained mixtures to retain their shape even at very early ages (right after mixing) after removal from molds. This further indicates that shape stability is an attribute of HPMC rather than cementitious compound hydration. Samples of the present study were tested up to 150 min after the first contact of water with Portland Cement. It has been observed that HPMC addition not only improves the early strength but also affects the rate of strength gain of these composites. Results show that up to 90 min, the green strength of all composites was improved in direct proportion to the dosage of HPMC. From 120–150 min, the trend seems to change in favor of lower HPMC content. Apparently, although no strength retrogression was observed, it is clear that higher HPMC dosage led to slower

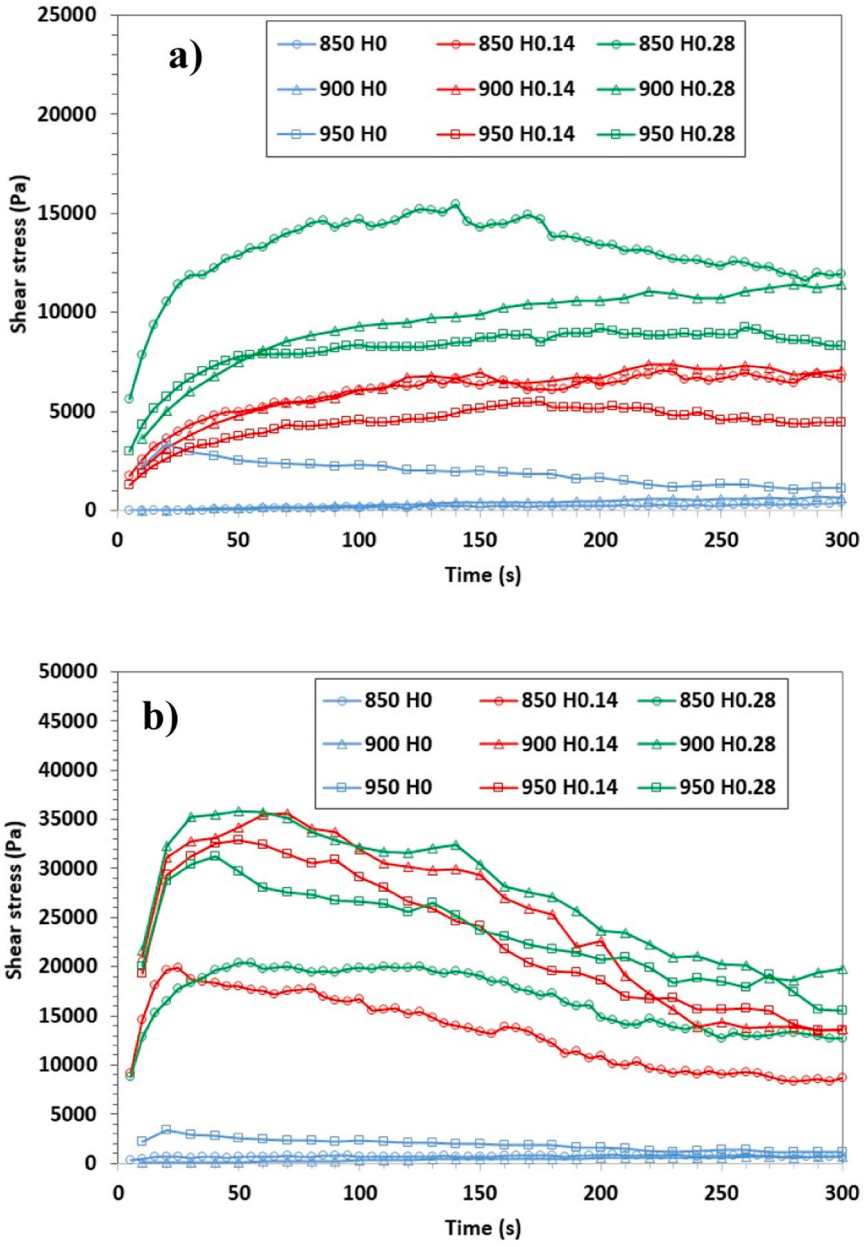

Fig. 17. Graphs of shear stress - time for mixtures for (a) early fresh age (15 min), (b) late age (30 min).

Table 6
Material flow parameters determined with the help of the Basterfield equation.

Parameter	850 H0.14	850 H0.28	900 H0.14	900 H0.28	950 H0.14	950 H0.28
k (kPa.s^n)	1.16	164.10	6.28	9.16	2.55	13.39
n	3.89	0.01	0.65	2.24	2.76	1.76
σ_o (kPa)[a]	20.66	−123.80	7.58	22.68	10.66	20.90
τ_0 (kPa)[a]	11.93	−71.48	4.37	13.09	6.15	12.07
R^2	1.00	0.98	1.00	1.00	1.00	1.00

[a] the negative static yield flow stress and shear yield stress values have been assumed to be zero.

strength gain rates. Slower strength gain rate in proportion to HPMC dosage can be attributed to the retardation of hydration by HPMC. In harmony with this finding, previous studies have reported that HPMC addition led to set retardation of cementitious composites [41]. Moreover, the findings of this study highlight the effect of aggregate volume on the green strength of these mixtures. It has been observed that at an equal W/C ratio, the green strength of the mixtures decreases as the cement dosage increases. In other words, the binder volume is inversely proportional to the green strength. The reason for this is the decrease in aggregate volume in the mix composition. The aggregate phase can act as a skeleton, increasing the green strength. However, the increase in aggregate volume can adversely affect the extrudability and bonding properties of these mixtures. Overall, the effect of HPMC dosage on green strength is slightly higher at early stages on mixtures with high cement dosages, but this trend becomes negligible with time. In other words, at an early age (20 min), increasing the HPMC dosage had an ignorable effect on the green strength of these mixtures, except for mixtures with 950 kg/m^3 cement dosage. Moreover, this green strength-enhancing effect of HPMC becomes unpronounced with time despite doubling the HPMC dosage.

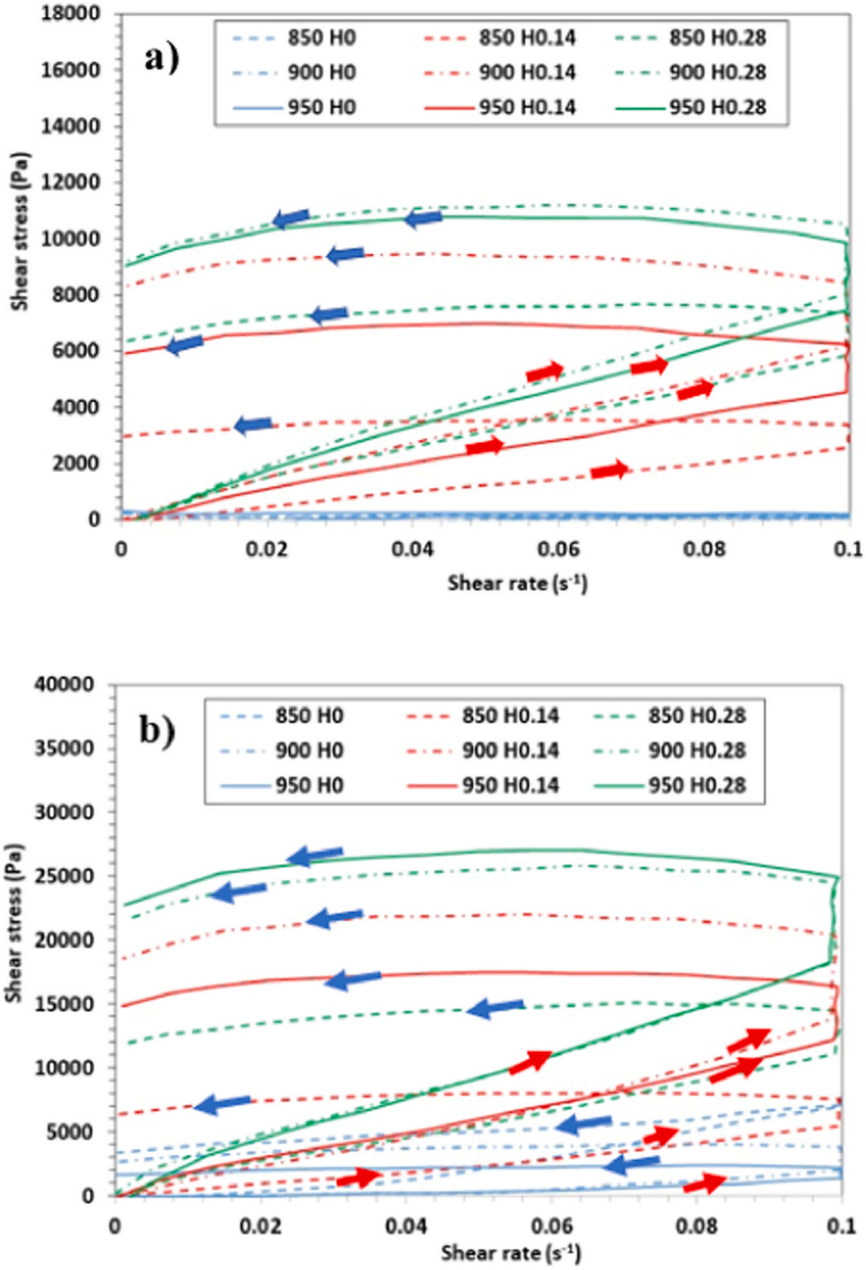

Fig. 18. Flow curve test results for mixtures for (a) early fresh age (15 min), (b) late age (30 min).

3.6. Hardened mechanical properties

3.6.1. Flexural strength

Fig. 27 presents the flexural strength values of developed 3D printable mortars concerning their curing period. Tests were performed on mold-cast specimens at 7 and 28 days of standard water curing at ambient temperature. Flexural strength decrement with HPMC addition is evident at both 7 and 28 days. Strength loss is observed in all mixtures regardless of their composition. Also, the loss in flexural strength increased with increasing HPMC content. However, this increase did not follow a linear pattern. This can be inferred by considering the loss in strength of up to 21.15 % for the mix with 850 kg/m^3 cement dosage due to a 0.14 % HPMC inclusion by weight of cement. However, By doubling HPMC's content from 0.14 % to 0.28 %, the strength loss increased slightly by 0.48 %. Similarly, the loss in strength with HPMC addition reached up to 23.9 % and 4.73 % for mix-900 kg/m^3 and 21.9 % and 0.19 % for mix-950 kg/m^3 at seven days. A similar trend was observed at 28 days for all investigated cement dosages, albeit at different values. The flexural strength values recorded at different cement dosages appeared close to each other. It can be associated with the fact that tested mixtures contained equal w/c ratios and were tailored to possess equal workability. Hence, their flexural strength values were more or less similar. Furthermore, it has been noticed that, unlike the compressive strength values, the flexural strength values of these mixtures did not increase with curing age. Their strength peaked at seven days but did not increase further at 28 days. The loss in strength by HPMC addition has been reported in previous studies [5,42]. It was reported that the addition of HPMC led to an increase in porosity, resulting in strength loss [42]. Furthermore, when the flexural strengths of mixtures 850 H0, 900 H0, and 950 H0 without HPMC are compared based on aggregate volumes, no effect of aggregate volume is observed on the 7 and 28 days.

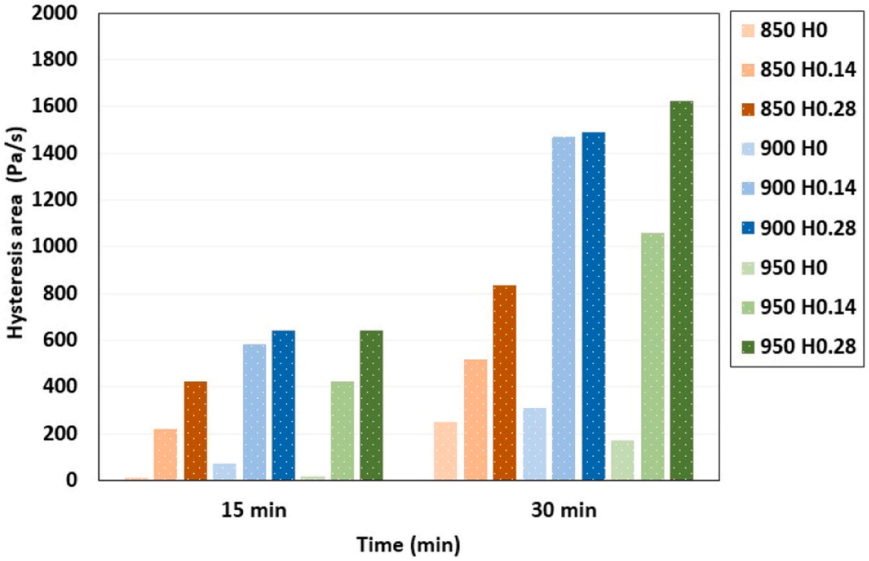

Fig. 19. Comparative plot of hysteresis areas of mixtures depending on HPMC dosage (t=15 min and t=30 min).

Table 7
Static and dynamic yield stress, plastic viscosities, and hysteresis areas of the mixtures (t= 15 min and 30 min).

MIXTURES	Static Yield Stress (Pa)		Dynamic Yield* Stress (Pa)		Plastic Viscosity* (mPa.s)		Hysteresis area* (Pa/s)	
	15 min	30 min	15 min	30 min	15 min	30 min	15 min	30 min
850 H0	389.91	867.18	100.52	3463.2	7.9074×10^5	115.56×10^5	−12.994	−250.21
850 H0.14	7063.9	19.858	3209.8	7052.1	38.48×10^5	118.12×10^5	−218.54	−516.79
850 H0.28	15.482	20.347	6845.6	12.749	94.428×10^5	274.57×10^5	−424.07	−837.06
900 H0	690.83	4178.0	8.1376	2992.8	2.3672×10^5	128.41×10^5	−7.3356	−309.78
900 H0.14	7642.2	35.579	9101.6	20.320	10.212×10^5	151.62×10^5	−582.8	−1472.2
900 H0.28	11.926	35.800	10.086	23.294	115.92×10^5	271.75×10^5	−643.42	−1489.4
950 H0	1098.1	3373.9	513.64	1815.4	12.293×10^5	64.681×10^5	−17.966	−172.76
950 H0.14	5512.9	32.876	6510.7	16,157	18.222×10^5	132.15×10^5	−423.26	−1057.8
950 H0.28	9233.3	31.217	9939.1	24.811	71.862×10^5	198.27×10^5	−642.51	−1624.1

* Bingham curve data

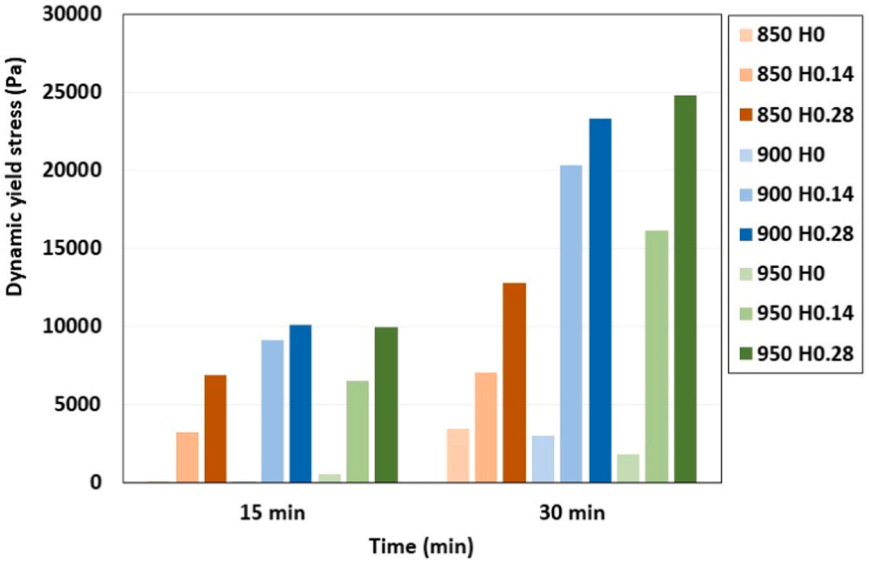

Fig. 20. Comparative graph of the dynamic yield stress of the mixtures depending on HPMC dosage (t=15 min and t=30 min).

3.6.2. Compressive strength

The compressive strength values of developed 3D printable mortars at 7 and 28 days are given in Fig. 28. The incorporation of HPMC led to a considerable loss in compressive strength values at 7 and 28 days. Nonetheless, it has been observed that despite the strength losses at both ages, no strength retrogression occurred with age in all mixtures. In other words, the intrinsic strength increment with the age of cementitious composites held true even after the addition of HPMC.

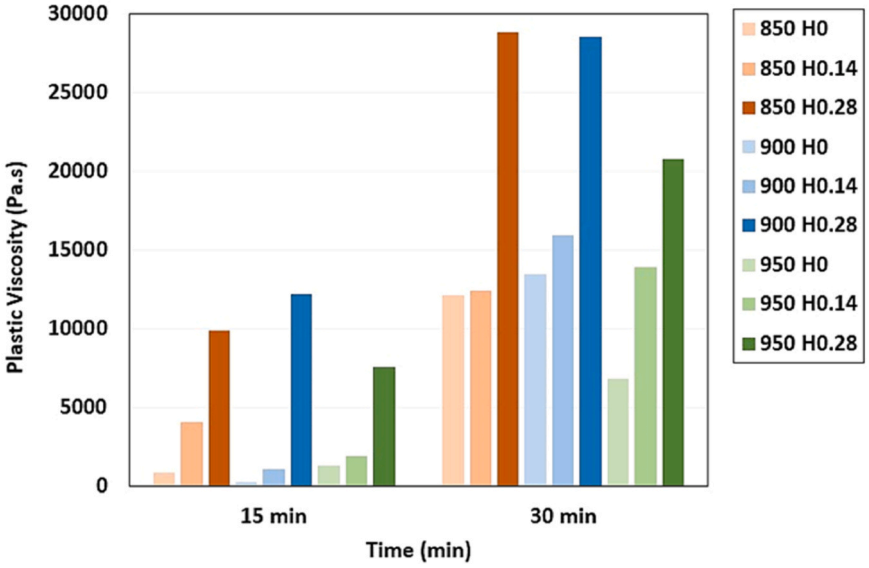

Fig. 21. Comparative graph of plastic viscosities of the mixtures depending on HPMC dosage (t=15 min and t=30 min).

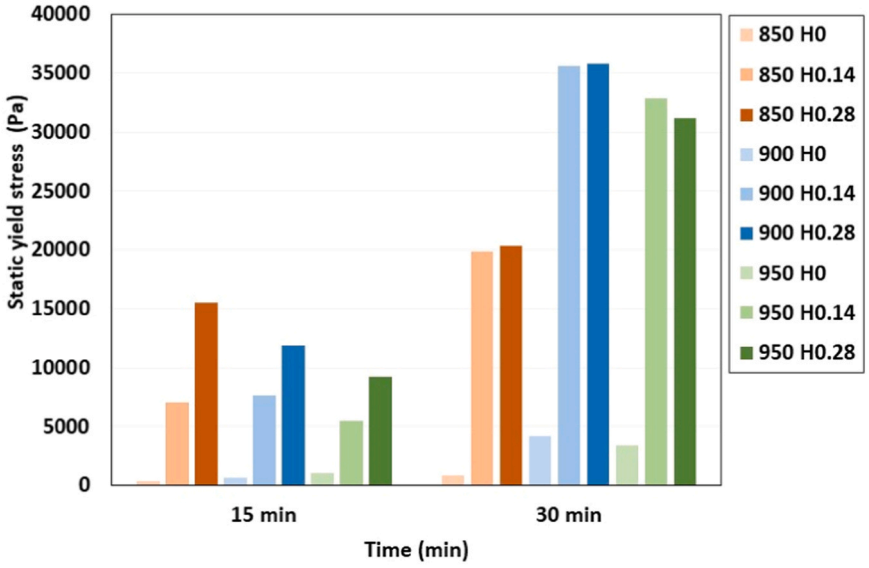

Fig. 22. Time-dependent comparison of the static yield stress of the mixtures.

Furthermore, it has been determined that although the loss in compressive strength was proportional to the dosage of HPMC in all mixtures, it did not follow a linear pattern. For instance, while the loss in compressive strength for samples with 850 kg/m^3 cement dosage at 0.14 % HPMC inclusion at 28 days reached up to 25.7 %, it increased only by 7 % when HPMC dosage was doubled. A similar trend holds true for all mixtures, albeit at different numbers. It has been observed that the loss in strength with HPMC addition grew larger with increasing binder volume, especially at seven days. When the strengths of HPMC-free samples are compared to the strength of samples with 0.14 % HPMC at 7 days for each investigated cement dosage, it can be seen that strength losses with HPMC addition increased with an increment in cement dosage or a decrease in aggregate volume. At this age, the loss in compressive strength of 26.4 %, 29.5 %, and 32.07 % was recorded for mixtures with 850, 900, and 950 kg/m^3 respectively. A similar trend was observed at 28-day compressive strengths with a slight exception for the mix with 950 kg/m^3.

The findings of the present study further confirm previously reported results in the literature on the effect of utilizing HPMC as a viscosity modifier in the development of cement-based 3D printable mixtures. It has been shown that HPMC inclusion led to higher porosity in the matrix. Similarly, the findings of this study further confirm the air-entraining effect of HPMC. Fig. 28 presents the unit weight of each mix before and after HPMC inclusion. As can be seen, the unit weight of the composites decreases as the dosage of HPMC increases, which can be attributed to the porosity increment caused by HPMC. Yalçınkaya [5] observed an increase in entrapped air and macropores caused by HPMC usage. An increase in porosity is known to adversely affect the strength of the cement-based composites. Hence, it can be concluded that the use of HPMC led to higher porosity and, subsequently, strength loss at both 7 and 28 days [5,42].

4. Conclusion

This study experimentally investigated the effect of various binder volumes and HPMC dosages on the fresh, rheological, and mechanical

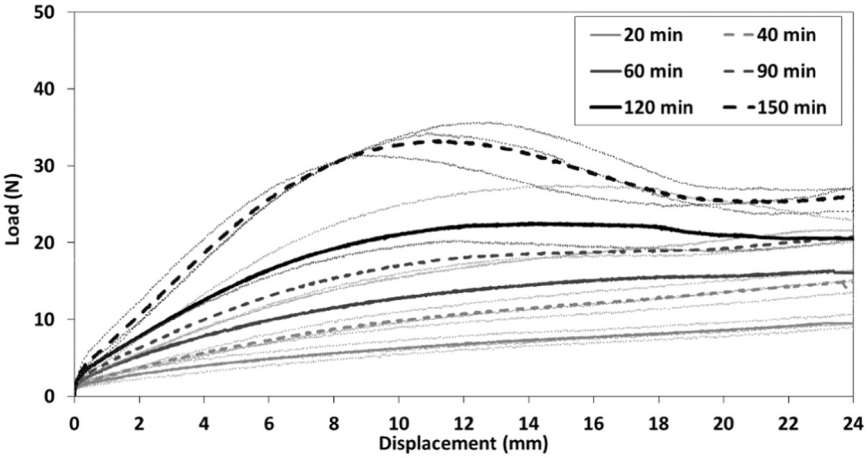

Fig. 23. A typical average load-displacement graph (900 H0.14 mixture).

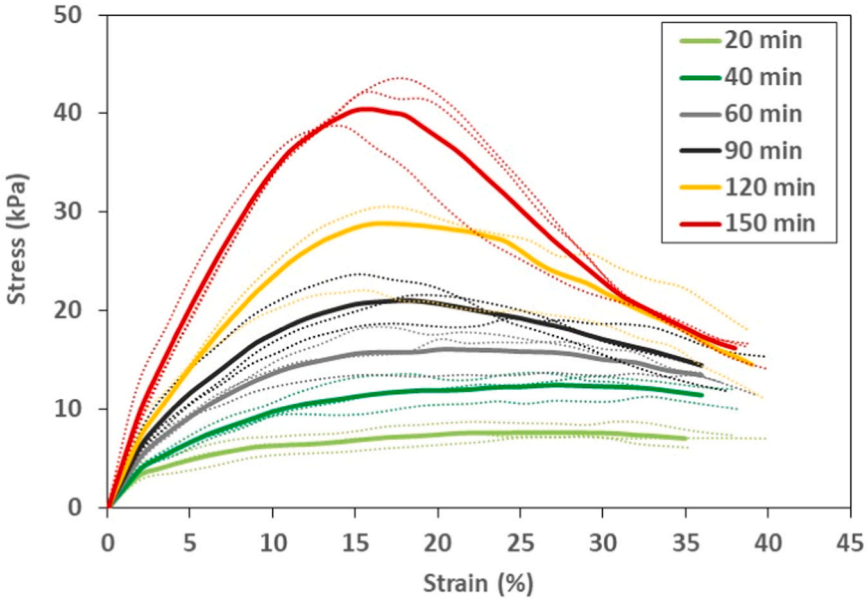

Fig. 24. A typical average stress-strain graph (900 H0.14 mixture).

properties of cement-based 3D printable mortars. Based on the findings of this study, the following conclusions can be made:

- At a constant W/C ratio, the green strength of the mixtures decreases as the cement dosage increases. The reason for this is the decrease in aggregate volume (44 %, 41 %, and 38 %) in the mix composition. The aggregate phase can act as a skeleton, increasing the green strength. Additionally, at an early age (20 min), the effect of HPMC dosage on green strength is more pronounced at a higher paste volume while being negligible at lower paste volumes. Moreover, the green strength enhancement induced by the increase in HPMC dosage becomes insignificant at later ages.
- HPMC addition positively affected the fresh properties of developed 3D printable mixtures, which enhanced extrudability, shape stability, and buildability. Furthermore, HPMC enhanced the extrudability at early ages by preventing segregation while considerably extending the extrudability window by preventing the water drainage from the mix during extrusion.
- The extrusion force of developed mixtures increases proportionately with the material age, nozzle length, material flow velocity, and HPMC dosage. However, from 120 min material age onwards, the trend is reversed owing to the set retarding effect of HPMC. Additionally, the effect of increasing the HPMC dosage was more pronounced on the extrudability at later ages at higher paste volumes (lower aggregate volume), allowing for extended extrudability windows.
- The addition of HPMC significantly enhanced the static yield stress, dynamic yield stress, and plastic viscosity in all mixtures. An increase in HPMC dosage further enhances these rheological properties, especially at an early age. The presence of HPMC provides a significant increase in static yield stress, depending on cement dosage. The addition of HPMC results in a more pronounced increase in the static yield stress at a lower paste volume. Furthermore, the increase in static yield stress with HPMC is not linear. The increase in static yield stress with time is somehow constant at higher and lower HPMC dosages. However, this increment varies in accordance with the aggregate volume in a directly proportional trend. In contrast, while the effect of HPMC dosage was pronounced in the early ages, it diminished with material age, indicating an optimal structuration rate at lower HPMC dosages.
- Increasing aggregate volume led to a decrease in compressive strength for the mixtures. On the other hand, HPMC addition

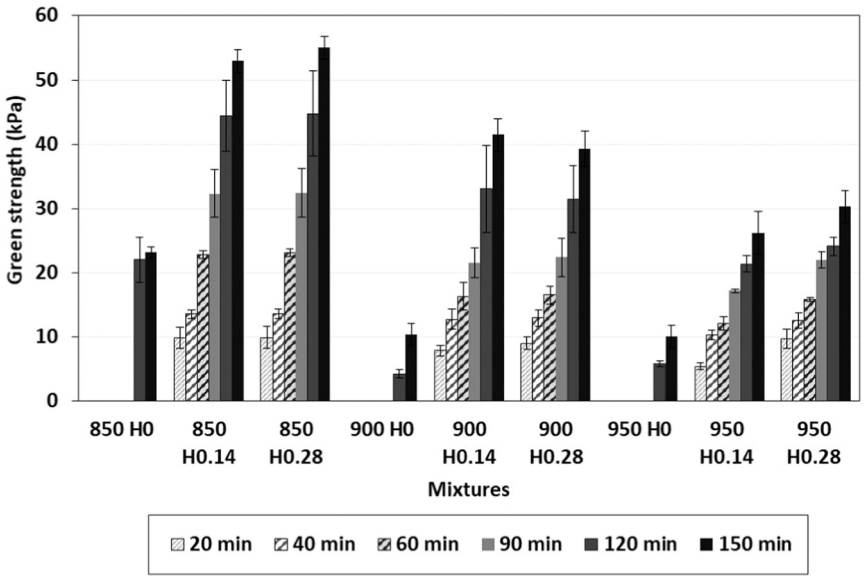

Fig. 25. Comparison of green strength development of the mixtures depending on HPMC dosage.

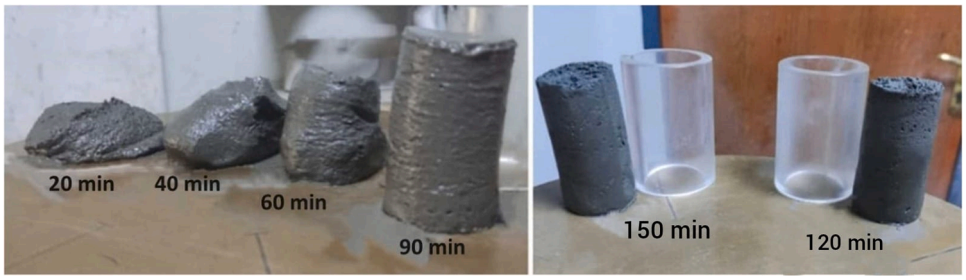

Fig. 26. Green strength measurements could not be taken at these ages due to the insufficient stability of the 950 H0 mixture when removed from the mold at t= 20, 40, and 60 min.

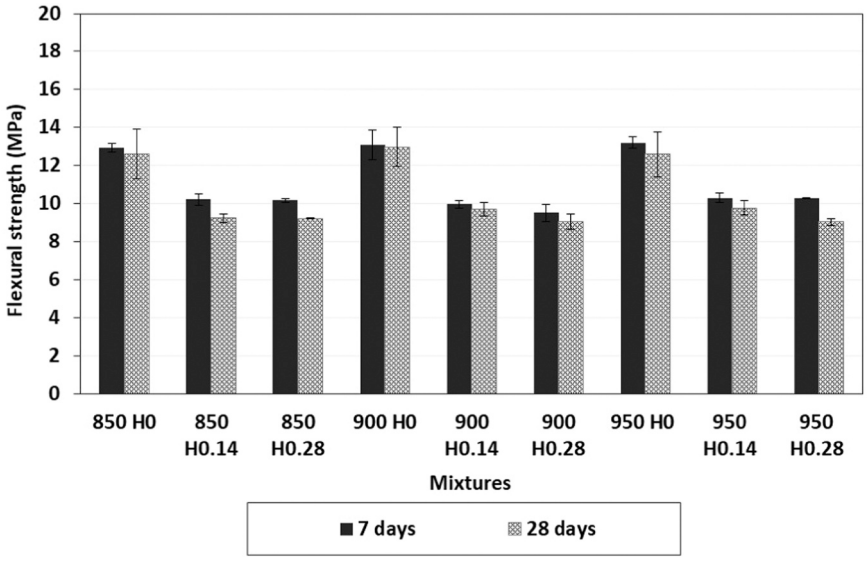

Fig. 27. Flexural strength of the mixtures.

adversely affected the compressive and flexural strengths, and this side effect could not be hindered by increasing the curing period. The increase in HPMC dosage led to increased loss of strength at the studied ages. Strength losses of up to 28.63 % and 32.7 % for flexural and compressive strength, respectively, were recorded.

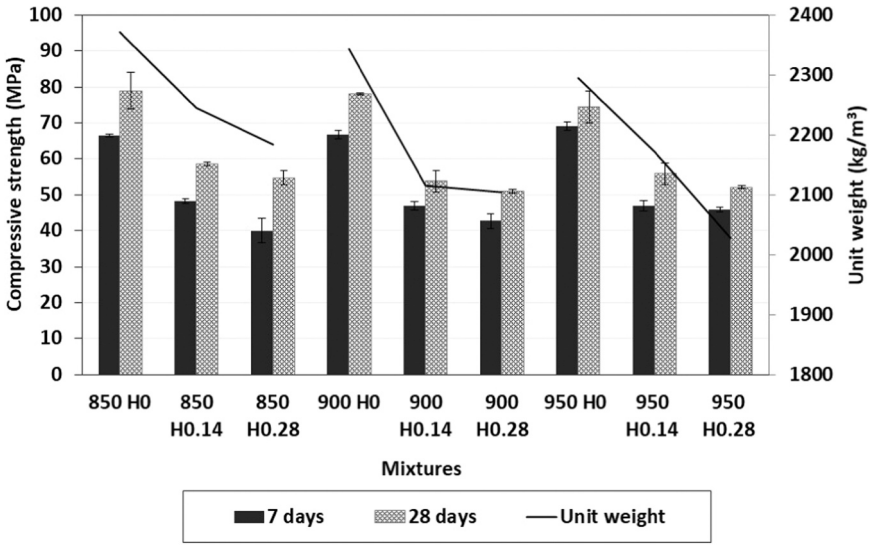

Fig. 28. Compressive strength and unit weight of the mixtures.

CRediT authorship contribution statement

Oğuzhan Çopuroğlu: Writing – review & editing, Supervision. **Halit Yazıcı:** Writing – review & editing, Resources. **Baraka Ciza:** Writing – review & editing, Writing – original draft, Visualization, Methodology, Investigation. **Ebru Kaya:** Writing – review & editing, Writing – original draft, Visualization, Methodology, Investigation. **Burak Felekoğlu:** Writing – review & editing, Resources, Methodology, Formal analysis. **Çağlar Yalçınkaya:** Writing – review & editing, Writing – original draft, Resources, Project administration, Funding acquisition, Formal analysis, Conceptualization.

Declaration of Competing Interest

The authors declare that they have no known competing financial interests or personal relationships that could have appeared to influence the work reported in this paper.

Acknowledgments

This study was supported by the Scientific and Technological Research Council of Türkiye (TÜBİTAK, Project no: 121M284). The authors gratefully acknowledge to TÜBİTAK. The second author, Ebru Kaya, thanks to YÖK 100/2000 Ph.D. Scholarship program. The authors would like to thank Limak Cement (Balıkesir Plant) for material support. And a special thanks to Ebru Sipahioğlu, Erdal Sarıtop, and Oğuz Kır for their help with material supply.

Declaration of conflicting interests

The author(s) declared no potential conflicts of interest with respect to the research, authorship, and/or publication of this article.

Data Availability

Data will be made available on request.

References

[1] T. Wangler, E. Lloret, L. Reiter, N. Hack, F. Gramazio, M. Kohler, M. Bernhard, B. Dillenburger, J. Buchli, N. Roussel, R. Flatt, Digital concrete: opportunities and challenges, RILEM Tech. Lett. 1 (2016) 67, https://doi.org/10.21809/rilemtechlett.2016.16.

[2] V. Mechtcherine, R. Buswell, H. Kloft, F.P. Bos, N. Hack, R. Wolfs, J. Sanjayan, B. Nematollahi, E. Ivaniuk, T. Neef, Integrating reinforcement in digital fabrication with concrete: a review and classification framework, Cem. Concr. Compos 119 (2021) 103964, https://doi.org/10.1016/j.cemconcomp.2021.103964.

[3] S. Hou, Z. Duan, J. Xiao, J. Ye, A review of 3D printed concrete: Performance requirements, testing measurements and mix design, Constr. Build. Mater. (2020) 121745, https://doi.org/10.1016/j.conbuildmat.2020.121745.

[4] V. Mechtcherine, F.P. Bos, A. Perrot, W.R.L. da Silva, V.N. Nerella, S. Fataei, R.J. M. Wolfs, M. Sonebi, N. Roussel, Extrusion-based additive manufacturing with cement-based materials – Production steps, processes, and their underlying physics: a review, Cem. Concr. Res 132 (2020) 106037, https://doi.org/10.1016/j.cemconres.2020.106037.

[5] Ç. Yalçınkaya, Influence of hydroxypropyl methylcellulose dosage on the mechanical properties of 3D printable mortars with and without fiber reinforcement, Buildings 12 (2022) 360, https://doi.org/10.3390/buildings12030360.

[6] A.U. Rehman, J.-H. Kim, 3D Concrete printing: a systematic review of rheology, mix designs, mechanical, microstructural, and durability characteristics, Materials 14 (2021) 3800, https://doi.org/10.3390/ma14143800.

[7] Z. Liu, M. Li, Y. Weng, T.N. Wong, M.J. Tan, Mixture design approach to optimize the rheological properties of the material used in 3D cementitious material printing, Constr. Build. Mater. 198 (2019) 245–255, https://doi.org/10.1016/j.conbuildmat.2018.11.252.

[8] S.C. Paul, G.P.A.G. van Zijl, I. Gibson, A review of 3D concrete printing systems and materials properties: current status and future research prospects, Rapid Prototyp. J. 24 (2018) 784–798, https://doi.org/10.1108/RPJ-09-2016-0154.

[9] N. Roussel, Rheological requirements for printable concretes, Cem. Concr. Res. 112 (2018) 76–85, https://doi.org/10.1016/j.cemconres.2018.04.005.

[10] Y. Chen, S. Chaves Figueiredo, Ç. Yalçinkaya, O. Çopuroğlu, F. Veer, E. Schlangen, The effect of viscosity-modifying admixture on the extrudability of limestone and calcined clay-based cementitious material for extrusion-based 3D concrete printing, Materials 12 (2019) 1374, https://doi.org/10.3390/ma12091374.

[11] A. Perrot, Y. Mélinge, D. Rangeard, F. Micaelli, P. Estellé, C. Lanos, Use of ram extruder as a combined rheo-tribometer to study the behaviour of high yield stress fluids at low strain rate, Rheol. Acta 51 (2012) 743–754, https://doi.org/10.1007/s00397-012-0638-6.

[12] R.A. Buswell, W.R. Leal de Silva, S.Z. Jones, J. Dirrenberger, 3D printing using concrete extrusion: a roadmap for research, Cem. Concr. Res 112 (2018) 37–49, https://doi.org/10.1016/j.cemconres.2018.05.006.

[13] T.T. Le, S.A. Austin, S. Lim, R.A. Buswell, A.G.F. Gibb, T. Thorpe, Mix design and fresh properties for high-performance printing concrete, (2012) 1221–1232. https://doi.org/10.1617/s11527-012-9828-z.

[14] Q. Yuan, Z. Li, D. Zhou, T. Huang, H. Huang, D. Jiao, C. Shi, A feasible method for measuring the buildability of fresh 3D printing mortar, Constr. Build. Mater. 227 (2019) 116600, https://doi.org/10.1016/j.conbuildmat.2019.07.326.

[15] E. Figueiredo, Stefan ChavesSchlangen, Effect of viscosity modifier admixture on Portland cement paste hydration and microstructure 212 (2019) 818–840, https://doi.org/10.1016/j.conbuildmat.2019.04.020.

[16] Y. Chen, Z. Li, S.C. Figueiredo, O. Çopuroğlu, F. Veer, E. Schlangen, Limestone and calcined clay-based sustainable cementitious materials for 3D concrete printing: a fundamental study of extrudability and early-age strength development, Appl. Sci. (Switz.) 9 (2019), https://doi.org/10.3390/app9091809.

[17] Y. Zhang, Y. Zhang, W. She, L. Yang, G. Liu, Y. Yang, Rheological and harden properties of the high-thixotropy 3D printing concrete, Constr. Build. Mater. 201 (2019) 278–285, https://doi.org/10.1016/j.conbuildmat.2018.12.061.

[18] M.K. Mohan, A.V. Rahul, K. Van Tittelboom, G. De Schutter, Rheological and pumping behaviour of 3D printable cementitious materials with varying aggregate content, Cem. Concr. Res. 139 (2021) 106258, https://doi.org/10.1016/j.cemconres.2020.106258.

[19] G.M. Moelich, J. Kruger, R. Combrinck, Plastic shrinkage cracking in 3D printed concrete, Compos B Eng. 200 (2020) 108313, https://doi.org/10.1016/j.compositesb.2020.108313.
[20] Standard Test Method for Flow of Hydraulic Cement Mortar., ASTM C1437-20, ASTM International: West Conshohocken, PA, USA (2020).
[21] J. Van Der Putten, M. Deprez, V. Cnudde, G. De Schutter, K. Van Tittelboom, Microstructural characterization of 3D printed cementitious materials, Materials 12 (2019), https://doi.org/10.3390/ma12182993.
[22] TS EN 480-2, TS EN 480-2; Admixtures for Concrete, Mortar and Grout—Test Methods—Part 2: Determination of Setting Time., 2008.
[23] X. Zhou, Z. Li, M. Fan, H. Chen, Rheology of semi-solid fresh cement pastes and mortars in orifice extrusion, Cem. Concr. Compos 37 (2013) 304–311, https://doi.org/10.1016/j.cemconcomp.2013.01.004.
[24] R.A. Basterfield, C.J. Lawrence, M.J. Adams, On the interpretation of orifice extrusion data for viscoplastic materials, Chem. Eng. Sci. 60 (2005) 2599–2607, https://doi.org/10.1016/j.ces.2004.12.019.
[25] H. Ogura, V.N. Nerella, V. Mechtcherine, Developing and testing of Strain-Hardening Cement-Based Composites (SHCC) in the context of 3D-printing, Materials 11 (2018) 1–18, https://doi.org/10.3390/ma11081375.
[26] R. Jayathilakage, P. Rajeev, J. Sanjayan, Yield stress criteria to assess the buildability of 3D concrete printing, Constr. Build. Mater. 240 (2020) 117989, https://doi.org/10.1016/j.conbuildmat.2019.117989.
[27] A. Perrot, D. Rangeard, V.N. Nerella, V. Mechtcherine, Extrusion of cement-based materials - an overview, RILEM Tech. Lett. 3 (2018) 91–97, https://doi.org/10.21809/rilemtechlett.2018.75.
[28] E.P. Koehler, D.W. Fowler, Development of a Portable Rheometer for Fresh Portland Cement Concrete, Aggregates Foundation for Technology, Research and Education (AFTRE), 2004.
[29] H. Ilcan, O. Sahin, A. Kul, E. Ozcelikci, M. Sahmaran, Rheological property and extrudability performance assessment of construction and demolition waste-based geopolymer mortars with varied testing protocols, Cem. Concr. Compos 136 (2023) 104891, https://doi.org/10.1016/j.cemconcomp.2022.104891.
[30] B. Panda, J.H. Lim, M.J. Tan, Mechanical properties and deformation behaviour of early age concrete in the context of digital construction, Compos B Eng. 165 (2019) 563–571, https://doi.org/10.1016/j.compositesb.2019.02.040.
[31] R.J.M. Wolfs, F.P. Bos, T.A.M. Salet, Early age mechanical behaviour of 3D printed concrete: numerical modelling and experimental testing, Cem. Concr. Res 106 (2018) 103–116, https://doi.org/10.1016/j.cemconres.2018.02.001.
[32] Y. Chen, S. Chaves Figueiredo, Z. Li, Z. Chang, K. Jansen, O. Çopuroğlu, E. Schlangen, Improving printability of limestone-calcined clay-based cementitious materials by using viscosity-modifying admixture, Cem. Concr. Res 132 (2020), https://doi.org/10.1016/j.cemconres.2020.106040.
[33] B. Zhu, B. Nematollahi, J. Pan, Y. Zhang, Z. Zhou, 3D concrete printing of permanent formwork for concrete column construction, Cem. Concr. Compos 121 (2021) 104039, https://doi.org/10.1016/j.cemconcomp.2021.104039.
[34] O.H. Wallevik, J.E. Wallevik, Rheology as a tool in concrete science: the use of rheographs and workability boxes, Cem. Concr. Res 41 (2011) 1279–1288, https://doi.org/10.1016/j.cemconres.2011.01.009.
[35] K.H. Khayat, Viscosity-enhancing admixtures for cement-based materials - An overview, Cem. Concr. Compos 20 (1998) 171–188, https://doi.org/10.1016/s0958-9465(98)80006-1.
[36] Y. Han, Z. Yang, T. Ding, J. Xiao, Environmental and economic assessment on 3D printed buildings with recycled concrete, J. Clean. Prod. 278 (2021) 123884, https://doi.org/10.1016/j.jclepro.2020.123884.
[37] S. Hou, Z. Duan, J. Xiao, J. Ye, A review of 3D printed concrete: performance requirements, testing measurements and mix design, Constr. Build. Mater. 273 (2021) 121745, https://doi.org/10.1016/j.conbuildmat.2020.121745.
[38] J. Kheir, A. Klausen, T.A. Hammer, L. De Meyst, B. Hilloulin, K. Van Tittelboom, A. Loukili, N. De Belie, Early age autogenous shrinkage cracking risk of an ultra-high performance concrete (UHPC) wall: modelling and experimental results, Eng. Fract. Mech. 257 (2021) 108024, https://doi.org/10.1016/j.engfracmech.2021.108024.
[39] J.G. Sanjayan, B. Nematollahi, M. Xia, T. Marchment, Effect of surface moisture on inter-layer strength of 3D printed concrete, Constr. Build. Mater. 172 (2018) 468–475, https://doi.org/10.1016/j.conbuildmat.2018.03.232.
[40] V.N. Nerella, S. Hempel, V. Mechtcherine, Effects of layer-interface properties on mechanical performance of concrete elements produced by extrusion-based 3D-printing, Constr. Build. Mater. 205 (2019) 586–601, https://doi.org/10.1016/j.conbuildmat.2019.01.235.
[41] G. Abbas, S. Irawan, S. Kumar, A.A.I. Elrayah, Improving oil well cement slurry performance using hydroxypropylmethylcellulose polymer, Adv. Mat. Res. (2013) 222–227, https://doi.org/10.4028/www.scientific.net/AMR.787.222.
[42] J. Pourchez, A. Peschard, P. Grosseau, R. Guyonnet, B. Guilhot, F. Vallée, HPMC and HEMC influence on cement hydration, Cem. Concr. Res 36 (2006) 288–294, https://doi.org/10.1016/j.cemconres.2005.08.003.
[43] K. Wang, C. Williams, W. Robert, Thixotropic behavior of cement-based materials: effect of clay and cement types Table of Contents, (2010).
[44] A. Perrot, D. Rangeard, Y. Mélinge, P. Estellé, C. Lanos, Extrusion criterion for firm cement-based materials, Appl. Rheol. 19 (2009), https://doi.org/10.3933/ApplRheol-19-53042.
[45] R. Jayathilakage, P. Rajeev, J. Sanjayan, Extrusion rheometer for 3D concrete printing, Cem. Concr. Compos 121 (2021) 104075, https://doi.org/10.1016/j.cemconcomp.2021.104075.
[46] N. Roussel, G. Ovarlez, S. Garrault, C. Brumaud, The origins of thixotropy of fresh cement pastes, Cem. Concr. Res. 42 (2012) 148–157, https://doi.org/10.1016/j.cemconres.2011.09.004.
[47] V.N. Nerella, M.A.B. Beigh, S. Fataei, V. Mechtcherine, Strain-based approach for measuring structural build-up of cement pastes in the context of digital construction, Cem. Concr. Res. 115 (2019) 530–544, https://doi.org/10.1016/j.cemconres.2018.08.003.
[48] R. Jayathilakage, P. Rajeev, J. Sanjayan, Rheometry for concrete 3D printing: a review and an experimental comparison, Buildings 12 (2022), https://doi.org/10.3390/buildings12081190.
[49] G. Lu, K. Wang, Theoretical and experimental study on shear behavior of fresh mortar, Cem. Concr. Compos 33 (2011) 319–327, https://doi.org/10.1016/j.cemconcomp.2010.09.002.
[50] A. Perrot, C. Lanos, Y. Melinge, P. Estellé, Mortar physical properties evolution in extrusion flow, Rheol. Acta 46 (2007) 1065–1073, https://doi.org/10.1007/s00397-007-0195-6.
[51] Y. Yin, J. Huang, T. Wang, R. Yang, H. Hu, M. Manuka, F. Zhou, J. Min, H. Wan, D. Yuan, B. Ma, Effect of Hydroxypropyl methyl cellulose (HPMC) on rheology and printability of the first printed layer of cement activated slag-based 3D printing concrete, Constr. Build. Mater. 405 (2023) 133347, https://doi.org/10.1016/j.conbuildmat.2023.133347.
[52] J. Xiao, S. Hou, Z. Duan, S. Zou, Rheology of 3D printable concrete prepared by secondary mixing of ready-mix concrete, Cem. Concr. Compos 138 (2023) 104958, https://doi.org/10.1016/j.cemconcomp.2023.104958.
[53] L. Patural, P. Marchal, A. Govin, P. Grosseau, B. Ruot, O. Devès, Cement and Concrete Research Cellulose ethers in fl uenceon water retention and consistency in cement-based mortars, Cem. Concr. Res. 41 (2011) 46–55, https://doi.org/10.1016/j.cemconres.2010.09.004.
[54] M. Sonebi, A. Perrot, Effect of mix proportions on rheology and permeability of cement grouts containing viscosity modifying admixture, Constr. Build. Mater. 212 (2019) 687–697, https://doi.org/10.1016/j.conbuildmat.2019.04.022.
[55] I. Ivanova, V. Mechtcherine, Effects of volume fraction and surface area of aggregates on the static yield stress and structural build-up of fresh concrete, Materials 13 (2020), https://doi.org/10.3390/ma13071551.